

A CAHN-HILLIARD MULTIPHASE SYSTEM WITH MOBILITIES FOR WETTING SIMULATION

ELIE BRETIN, ROLAND DENIS, SIMON MASNOU, ARNAUD SENGERS, AND GARRY TERII

ABSTRACT. This paper tackles the simulation of the wetting phenomenon using a phase field model. To this end, we extend to multiphase the Cahn-Hilliard model with doubly degenerate mobilities we introduced in [17] and we show that this extension still preserves the second order of approximation of the sharp limit. In a second part, we propose a simple and efficient numerical schemes that require only about 60 lines in **Matlab**. We then provide some numerical experiments illustrating the influence of mobility and surface tension coefficients. Finally, we explain how to apply our phase field model to approximate the wetting of a thin tube on different solid supports. .

1. INTRODUCTION

This paper concerns the approximation of the wetting or dewetting phenomenon that describes the evolution of a liquid phase on a fixed solid surface as a multiphase surface diffusion flow with mobilities in the phase field context. Recall that two centuries ago, Young [76] established the optimal shape of the liquid phase and prescribed the following contact angle θ formed by the liquid on the solid

$$\cos(\theta) = \frac{\sigma_{SV} - \sigma_{LS}}{\sigma_{VL}},$$

where $\sigma_{SV}, \sigma_{LS}, \sigma_{VL}$ represent respectively the surfaces tensions of the interfaces Solid-Vapor Γ_{SV} , Liquid-Solid Γ_{LS} and Vapor-Liquid Γ_{VL} . Mathematically, Young's law can be derived by minimizing the total energy in the solid-liquid-vapor system. If we ignore gravity, the total energy reads

$$\mathcal{E} = \sigma_{SV}\mathcal{H}^{d-1}(\Gamma_{SV}) + \sigma_{LS}\mathcal{H}^{d-1}(\Gamma_{LS}) + \sigma_{VL}\mathcal{H}^{d-1}(\Gamma_{VL}),$$

which can be reformulated using a generic L -phase perimeter

$$(1) \quad P(\Omega_1, \dots, \Omega_L) = \frac{1}{2} \sum_{i,j=1}^L \sigma_{i,j} \mathcal{H}^{d-1}(\Gamma_{i,j}),$$

where $\Omega \subset \mathbb{R}^d$ is an open domain divided into the partition of closed subsets $(\Omega_1, \Omega_2, \dots, \Omega_L)$. Here $\Gamma_{i,j}$ and $\sigma_{i,j}$ are respectively the interface and the surface tension between phase i and j . We also assume that the surface tensions are strictly positives $\sigma_{i,j} > 0$ and satisfy the triangular inequality

$$\sigma_{i,j} + \sigma_{j,k} \geq \sigma_{i,k} \quad \text{for any } i, j, k,$$

to ensure the lower semi-continuity of the associated L -phase perimeter [55, 52, 21].

The evolution of the physical system can then be approximated by a multiphase surface diffusion flow. This motion can be viewed as the H^{-1} gradient flow of (1) which ensure its decay while maintaining the volume of each phase locally. In particular, the normal velocity V_{ij} at the interface Γ_{ij} reads as

$$\frac{1}{\nu_{ij}} V_{ij} = \sigma_{ij} \Delta_{\Gamma_{ij}(t)} H_{ij}(t),$$

2020 *Mathematics Subject Classification.* 74N20, 35A35, 53E10, 53E40, 65M32, 35A15.

Key words and phrases. Phase field approximation, Cahn-Hilliard equation, surface diffusion, degenerate mobilities, numerical approximation.

where $H_{ij}(t)$ denotes the scalar mean curvature on $\Gamma_{ij}(t)$, $\Delta_{\Gamma_{ij}(t)}$ the Laplace-Beltrami operator defined on the surface and $\nu_{ij} \geq 0$ the surface mobility coefficients.

In the case of wetting or dewetting simulation, it corresponds to use $L = 3$ phases, the liquid Ω_L , the solid Ω_S and the vapor Ω_V . Moreover, as the surface tension coefficients $(\sigma_{LV}, \sigma_{SV}, \sigma_{SL})$ satisfy the triangle inequality assumption, it gives the existence of three positive coefficients $\sigma_L, \sigma_S, \sigma_V$ such as

$$\sigma_{LV} = \sigma_L + \sigma_V, \quad \sigma_{SV} = \sigma_S + \sigma_V \quad \text{and} \quad \sigma_{SL} = \sigma_S + \sigma_L.$$

About the surface mobilities, we can also take

$$(\nu_{LV}, \nu_{SV}, \nu_{SL}) = (1, 0, 0),$$

in order to fix the solid phase. This set of coefficients is then harmonically additives in the sense that it exists three positive coefficients ν_S, ν_L and ν_V such as

$$\nu_{LV}^{-1} = \nu_L^{-1} + \nu_V^{-1}, \quad \nu_{SV}^{-1} = \nu_S^{-1} + \nu_V^{-1} \quad \text{and} \quad \nu_{SL}^{-1} = \nu_S^{-1} + \nu_L^{-1}.$$

Indeed, we can just consider $\nu_S = 0$ and $\nu_L = \nu_V = 2$.

Having in mind this kind of applications, we assume in the rest of the paper that the surface tensions are additives, i.e. there exists $\sigma_i \geq 0$ such that $\sigma_{ij} = \sigma_i + \sigma_j$. We also assume that the mobility coefficients are also harmonically additives given the existence of some positive coefficients ν_i satisfying $\nu_{ij}^{-1} = \nu_i^{-1} + \nu_j^{-1}$.

The advantage is that it is possible to reformulate the partition of the perimeter in the more convenient following form

$$(2) \quad P(\Omega_1, \Omega_2, \dots, \Omega_L) = \sum_{i=1}^L \sigma_i P(\Omega_i)$$

which can be approximated by a sum of scalar Cahn Hilliard energies

$$P_\varepsilon(\mathbf{u}) = \begin{cases} \frac{1}{2} \sum_{k=1}^L \sigma_k \int_{\Omega} \left(\frac{\varepsilon}{2} |\nabla u_k|^2 + \frac{1}{\varepsilon} W(u_k) \right) dx, & \text{if } \sum_{k=1}^L u_k = 1 \\ +\infty & \text{otherwise} \end{cases}$$

where $\mathbf{u} = (u_1, u_2, \dots, u_L) \in \mathbb{R}^L$, ε is a small parameter that characterizes the width of the diffuse interface, and $W(s) = \frac{s^2(1-s)^2}{2}$ is a double-well potential.

A natural idea to approximate the multiphase surface diffusion flow should be to consider the H^{-1} gradient flow of P_ε which yields the following Cahn-Hilliard system

$$\begin{cases} \varepsilon^2 \partial_t u_k = \nu_k \Delta (\sigma_k \mu_k + \lambda) \\ \mu_k = W'(u_k) - \varepsilon^2 \Delta u_k, \end{cases}$$

where λ is the Lagrange multiplier associated to the partition constraint $\sum u_k = 1$. Here, we follow the idea of [14] in the treatment of the mobility $\nu_{i,j}$ which explicitly requires its harmonic additive decomposition.

However, the asymptotic expansion of this phase field system is not clear and to the limit of our knowledge, there is not proof which gives an analysis of its convergence. The main obstacle to overcome is the non local nature of the system, especially in the multiphase case.

In [17], we reviewed different Cahn-Hilliard systems in the two phase case and proposed a new one. Essentially, they revolve around the use of degenerate mobilities that vanish in pure phase regions. Such terms localize the system and allow to prove asymptotic results. In the next paragraph we sum up the properties and choices of parameters of biphasic case which we will extend to the multiphase case. We refer to [17] for details.

Recall that [57, 4] proved that the classical Cahn-Hilliard equation

$$\begin{cases} \varepsilon^2 \partial_t u = \Delta \mu, \\ \mu = W'(u) - \varepsilon^2 \Delta u, \end{cases}$$

does not converge to surface diffusion flow but rather to the Hele-Shaw model which is not local. Cahn et al. [20] then introduced a new system by adding a concentration-dependent mobility M . It is often referred as degenerate mobility in the sense that no motion occurs in the pure states regions. They obtained the following equation that we will refer to as **MCH** :

$$\begin{cases} \varepsilon^2 \partial_t u = \operatorname{div} (M(u) \mu), \\ \mu = W'(u) - \varepsilon^2 \Delta u. \end{cases}$$

They managed to obtain a formal convergence to the correct motion. However, they used a logarithmic potential which can raise some numerical issues. The potential commonly chosen in the literature and the one that we will use for the remainder of this paper is the smooth potential

$$W(s) = \frac{1}{2} s^2 (1 - s)^2.$$

The choice of the mobility M has been discussed theoretically in [37, 44, 45]. It is proven by a formal asymptotic method that the choice $M(u) = u(1 - u)$ does not lead to the correct velocity as an additional bulk diffusion term appears. These conclusions have been corroborated numerically in [27, 28] where undesired coarsening effects are observed. Therefore a second order mobility $M(u) = u^2(1 - u)^2$ is required to recover the correct velocity. These conclusions have been extended to the anisotropic case in [32]. From now on, we fix

$$M(s) = s^2(1 - s)^2.$$

While model **MCH** has the correct sharp interface limit and produces satisfactory numerical results, it has a well identified drawback. In the asymptotic, the leading error term is of order 1 and becomes relevant when reaching the pure states 0, 1, causing oscillations and an imprecise profile for the solution. The problem is two-fold. Firstly, the solution does not remain within the physical range of $[0, 1]$, which means that in the multiphase context, some phases might not be positive in some areas. Secondly, this induces some numerical volume losses despite the natural volume preservative nature of the Cahn-Hilliard equation as illustrated in [17].

In [58], the authors managed to improve the numerical accuracy by introducing another degeneracy in the model. It has been successfully adapted in various applications, see for example [2, 56, 60, 59]. Despite its numerical property, the aforementioned model does not derive from an energy. It is thus more difficult to prove rigorously theoretical properties and to extend the model to complex multiphase applications. Therefore, a variational adaptation has been proposed in [62] where the second degeneracy is injected in the energy. Because it relies on modifying the energy, it makes it more complex to extend to complex multiphase applications or to add an anisotropy.

In [17], we proposed a different approach where the additional mobility N was incorporated in the metric of the gradient flow instead of the geometry of the evolution problem. The so-called model **NMNCH** reads

$$\begin{cases} \varepsilon^2 \partial_t u &= N(u) \operatorname{div} (M(u) \nabla (N(u) \mu)) \\ \mu &= W'(u) - \varepsilon^2 \Delta u, \end{cases}$$

The presence of two additional terms $N(u)$ is needed to ensure the variational nature of the model. Following formal asymptotic, we then identified the correct choice for N to be

$$N(s) = \frac{1}{\sqrt{M(s)}} = \frac{1}{s(1 - s)}.$$

Indeed, it allows to nullify the error term of order 1 in the solution, making the model **NMNCH** of order 2. The profile obtained for solution u is very precise and the volume conservation is ensured up to an order 2 (order 1 for **MCH**).

Concerning the positivity property, we observed in the biphasic case a better numerical accuracy from model **NMNCH** than from model **MCH**. While there is still an overshoot of the solution that goes beyond the physical range when reaching the pure states, it is of order $\mathcal{O}(\varepsilon^2)$ rather than $\mathcal{O}(\varepsilon)$.

In this paper, we propose to extend the models **MCH** and **NMNCH** to the case of L phases. From the modeling viewpoint, this amounts to add the influence of surface tensions σ_{ij} and phase mobilities ν_{ij} . To this end, we adapt the work of [14] done for the Allen-Cahn system to the Cahn-Hilliard system. In particular, we propose to give an analysis the two following phase field models:

- The **MCH** multiphase field model:

$$(3) \quad \begin{cases} \varepsilon^2 \partial_t u_k = \nu_k \operatorname{div} (M(u_k) \nabla (\sigma_k \mu_k + \lambda)) , \\ \mu_k = W'(u_k) - \varepsilon^2 \Delta u_k , \end{cases}$$

with the mobility $M(s) = 2W(s)$.

- The **NMNCH** multiphase field model

$$(4) \quad \begin{cases} \varepsilon^2 \partial_t u_k = \nu_k N(u_k) \operatorname{div} (M(u_k) \nabla (\sigma_k N(u_k) \mu_k + \lambda)) , \\ \mu_k = W'(u_k) - \varepsilon^2 \Delta u_k . \end{cases}$$

with the mobilities $M(s) = 2W(s)$ and $N(s) = 1/\sqrt{M(s)}$.

Notice that in each case, λ is the Lagrangian multiplier encoding the partition constraint $\sum_{k=1}^L u_k = 1$.

1.1. Outline of this paper.

In a first section, we first gives a formal asymptotic analysis of the **MCH** and **NMNCH** multiphase model. In particular, we show that the limit law of each model corresponds well to the multiphase surface diffusion flow with the advantage for the second one to be of order 2 in ε . In a second numerical section, we first introduce a numerical scheme based on the Fourier-spectral convex-concave semi implicit approach in the same spirit of [35, 17]. We then gives some numerical experiments which illustrate the stability of our scheme and the asymptotic properties of the two phase field models. In the last section, we consider the special case of wetting and dewetting phenomenon for which, we derive a simplified model using the liquid phase only. We then shows some numerical experiments en 3D, using smooth and rough surfaces and different Young angle conditions.

2. FORMAL MATCHED ASYMPTOTIC

In this section, we demonstrate the two following results 1 and 2 via formal matched asymptotic. Here, we introduce the function q is the so-called *optimal profile* associated with the potential W and defined by the equation $q'(z) = -\sqrt{2W(q(z))}$. In the case where $W(s) = \frac{1}{2}s^2(1-s)^2$, this profile reads as

$$q(z) = \frac{1 - \tanh(\frac{z}{2})}{2}.$$

We also need to introduce the following constants

$$c_W = \int_{\mathbb{R}} (q'(z))^2 dz, \quad c_M = \int_{\mathbb{R}} M(q(z)) dz \quad \text{and} \quad c_N = \int_{\mathbb{R}} \frac{q'(z)}{N(q(z))} dz.$$

We can now state results 1 and 2 concerning the properties of models **MCH** and **NMNCH**.

Result 1. *The solution \mathbf{u}^ε of the **MCH** model*

$$\begin{cases} \varepsilon^2 \partial_t u_k = \nu_k \operatorname{div} (M(u_k) \nabla (\sigma_k \mu_k + \lambda)), \\ \mu_k = W'(u_k) - \varepsilon^2 \Delta u_k, \end{cases}$$

satisfies near the interface Γ_{ij}^ε the following asymptotic expansion

$$\begin{cases} u_i^\varepsilon = q \left(\frac{\operatorname{dist}(x, \Omega_i^\varepsilon)}{\varepsilon} \right) + \mathcal{O}(\varepsilon), \\ u_j^\varepsilon = 1 - q \left(\frac{\operatorname{dist}(x, \Omega_i^\varepsilon)}{\varepsilon} \right) + \mathcal{O}(\varepsilon), \\ u_k^\varepsilon = \mathcal{O}(\varepsilon). \end{cases}$$

Here dist denotes the signed distance function and $\Omega_i^\varepsilon = \{u_i^\varepsilon \geq 1/2\}$. Moreover, the normal velocity V_{ij}^ε at the interface Γ_{ij}^ε is given by:

$$\frac{1}{\nu_{ij}} V_{ij}^\varepsilon = \sigma_{ij} c_M c_W \Delta_\Gamma H_{ij} + \mathcal{O}(\varepsilon).$$

Result 2. *The solution \mathbf{u}^ε of the **NMNCH** model*

$$\begin{cases} \varepsilon^2 \partial_t u_k = \nu_k N(u_k) \operatorname{div} (M(u_k) \nabla (\sigma_k N(u_k) \mu_k + \lambda)), \\ \mu_k = W'(u_k) - \varepsilon^2 \Delta u_k, \end{cases}$$

satisfies near the interface Γ_{ij}^ε the following asymptotic expansion

$$\begin{cases} u_i^\varepsilon = q \left(\frac{\operatorname{dist}(x, \Omega_i^\varepsilon)}{\varepsilon} \right) + \mathcal{O}(\varepsilon^2), \\ u_j^\varepsilon = 1 - q \left(\frac{\operatorname{dist}(x, \Omega_i^\varepsilon)}{\varepsilon} \right) + \mathcal{O}(\varepsilon^2), \\ u_k^\varepsilon = \mathcal{O}(\varepsilon^2), \end{cases}$$

where Ω_i^ε is still defined by $\Omega_i^\varepsilon = \{u_i^\varepsilon \geq 1/2\}$. Moreover, the normal velocity V_{ij}^ε at the interface Γ_{ij}^ε is given by:

$$\frac{1}{\nu_{ij}} V_{ij}^\varepsilon = \sigma_{ij} \frac{c_W c_M}{(c_N)^2} \Delta_\Gamma H_{ij} + \mathcal{O}(\varepsilon).$$

In this section, we then first recall the tools necessary for our derivations presented for the model **MCH**, following the notations of [3, 24, 16]. The proof is given in dimension 2 only for the sake of simplicity of notations and readability. We first perform the actual asymptotic for **MCH** model. We end up with the **NMNCH** model, which we have to rewrite to avoid indeterminate forms. For the most part, the calculations remain the same as for the biphasic case presented in [17].

2.1. Formal asymptotic toolbox.

In this multiphase context, we study the behavior of the system in two regions: near the interface Γ_{ij} separating two given phases i and j and far from it. We denote u_k the solution for a random phase k . Whether k can designate i and j in a equation will be clear from the context.

To derive the method we require that the interface $\Gamma(t, \varepsilon)$ remains smooth enough and that there exists a neighborhood

$$\mathcal{N} = \mathcal{N}_{ij}^\delta(\Gamma(t, \varepsilon)) = \{x \in \Omega / |d(x, t)| < 3\delta\},$$

in which the signed distance function $d := d_{ij}$ to the interface Γ_{ij} is well-defined. \mathcal{N} is called the *inner region* near the interface and its complement the *outer region*.

Outer variables:

Far from the interface, we consider the *outer functions* (u_k, μ_k) depending on the standard *outer variable* x . The systems remain the same, namely for **MCH**:

$$(5) \quad \begin{cases} \varepsilon^2 \partial_t u_k = \nu_k \operatorname{div}(M(u_k) \nabla(\sigma_k \mu_k + \lambda)), \\ \mu_k = -\varepsilon^2 \Delta u_k + W'(u_k). \end{cases}$$

Inner variables:

Inside \mathcal{N} we define the *inner functions* (U_k, μ_k) depending on the *inner variables* (z, s) , where z is the variable along the normal and s is the variable in the direction of the arc-length parameterization S of the interface Γ :

$$\begin{cases} U_k(z, s, t) := U_k\left(\frac{d(x, t)}{\varepsilon}, S(x, t), t\right) = u(x, t), \\ \mu_k(z, s, t) := \mu_k\left(\frac{d(x, t)}{\varepsilon}, S(x, t), t\right) = \mu_k(x, t). \end{cases}$$

In order to express the derivatives U_k , we first need to calculate the gradient and the Laplacian of d and S . The properties of d are common knowledge in differential geometry:

$$\begin{cases} \nabla d(x, t) = n(x, t), \\ \Delta d(x, t) = \sum_{l=1}^{d-1} \frac{\kappa_l(\pi(x))}{1 + \kappa_l(\pi(x))d(x, t)} = \frac{H}{1 + \varepsilon z H} \text{ in dimension 2.} \end{cases}$$

where π is the projection on Γ and κ_k the principal curvatures.

Let $X_0(s, t)$ be a given point of the interface Γ_{ij} and $X(z, s, t)$ the point inside \mathcal{N} such that its projection on the interface is X_0 . Then, the expression of X is

$$X(z, s, t) = X_0(s, t) + \varepsilon z n(s, t).$$

Deriving the equation connecting the variable s and the function S gives:

$$s = S(X_0(s, t) + \varepsilon z n(s, t), t).$$

Then, deriving this equation with respect to z leads to

$$0 = \varepsilon n \cdot \nabla S = \varepsilon \nabla d \cdot \nabla S.$$

This means that there are no cross derivative terms. Moreover, the derivation of the same equation with respect to s gives

$$1 = (\partial_s X_0 + \varepsilon z H \partial_s n) \cdot \nabla S = (1 + \varepsilon z H) \tau \cdot \nabla S.$$

We know that ∇S is orthogonal to n , which means that it is collinear to the tangent τ and

$$\nabla S = \frac{\tau}{1 + \varepsilon z H}.$$

Taking the divergence, we find ΔS :

$$\begin{aligned} \Delta S &= \operatorname{div}\left(\frac{\tau}{1 + \varepsilon z H}\right) = \nabla\left(\frac{1}{1 + \varepsilon z H}\right) \cdot \tau + \frac{1}{1 + \varepsilon z H} \operatorname{div}(\tau), \\ &= \frac{1}{1 + \varepsilon z H} \partial_s \left(\frac{1}{1 + \varepsilon z H}\right) + \frac{1}{1 + \varepsilon z H} \tau \cdot \partial_s \tau, \\ &= -\frac{\varepsilon z \partial_s H}{(1 + \varepsilon z H)^3}. \end{aligned}$$

To express the connection between the derivatives of U_k, μ_k and u_k, μ_k , we come back to the definition of the inner functions:

$$u_k(x, t) = U_k\left(\frac{d(x, t)}{\varepsilon}, S(x, t), t\right).$$

Successive derivations according x give the following equations:

$$\begin{cases} \nabla u_k = \nabla d \frac{1}{\varepsilon} \partial_z U_k + \nabla S \partial_s U_k, \\ \Delta u_k = \Delta d \frac{1}{\varepsilon} \partial_z U_k + \frac{1}{\varepsilon^2} \partial_{zz} U_k + \Delta S \partial_s U_k + |\nabla S|^2 \partial_{ss} U_k, \\ \operatorname{div} (M(u_k) \nabla (N(u_k) \mu_k)) = \frac{1}{\varepsilon^2} (\partial_z M_k \partial_z (N_k \mu_k)) + \frac{M_k}{\varepsilon} \Delta d \partial_z (N_k \mu_k), \\ \quad + |\nabla S|^2 \partial_s (M_k \partial_s (N_k \mu_k)) + \Delta S M_k \partial_s (N_k \mu_k). \end{cases}$$

The *inner system* of the model **MCH** near the interface Γ_{ij} finally reads:

$$\begin{cases} \frac{\varepsilon^2}{\nu_k} (\partial_t U_k + \partial_t S \partial_s U_k) - \frac{\varepsilon}{\nu_k} V_{ij} \partial_z U_k = \frac{1}{\varepsilon^2} \partial_z (M(U_k) \partial_z (\sigma_k \mu_k + \Lambda)), \\ \quad + \frac{M(U_k)}{\varepsilon} \partial_z (\sigma_k \mu_k + \Lambda) \Delta d_{ij} + T_1(s), \\ \mu_k = W'(U_k) - \partial_{zz} U_k + \varepsilon \Delta d_{ij} \partial_z U_k + \varepsilon^2 T_2(s), \\ \Delta d_{ij} = \frac{H_{ij}}{1 + \varepsilon z H_{ij}} = H_{ij} - \varepsilon z H_{ij}^2 + \mathcal{O}(\varepsilon^2), \\ T_1(s) = \frac{\partial_s (M(U_k) \partial_s (\sigma_k \mu_k + \Lambda))}{(1 + \varepsilon z H_{ij})^2} - \frac{M(U_k) \varepsilon z \partial_s H_{ij}}{(1 + \varepsilon z H_{ij})^3} \partial_s (\sigma_k \mu_k + \Lambda), \\ T_2(s) = \frac{1}{(1 + \varepsilon z H)^2} \partial_{ss} U_k - \frac{\varepsilon z \partial_s H_{ij}}{(1 + \varepsilon z H_{ij})^3} \partial_s U_k. \end{cases}$$

Note that the terms in T_1 and T_2 are high order tangential terms that only play a role at the fourth order in the asymptotic.

Independence in z of the normal velocity V_{ij} :

The normal velocity of the interface $V_{ij}(s, t)$ is defined by:

$$V_{ij}(s, t) = \partial_t X_0(s, t) \cdot n(s, t).$$

In the neighborhood \mathcal{N} , we have the following property (which is a direct consequence of the definition of the signed distance function):

$$d(X_0(s, t) + \varepsilon z n(s, t), t) = \varepsilon z.$$

Deriving this with respect to t yields:

$$V_{ij}(s, t) = \partial_t X_0(s, t) \cdot \nabla d(X_0(s, t) + \varepsilon z n(s, t), t) = -\partial_t d(X(z, s, t), t).$$

Thus, the function $\partial_t d(x, t)$ is independent of z and we can extend the function everywhere in the neighborhood by choosing

$$V_{ij}(X_0(s, t) + \varepsilon z n, t) := -\partial_t d(X_0(s, t) + \varepsilon z n, t) = V_{ij}(s, t).$$

This property of independence is crucial to be able to extract the velocity from integrals in z in the following derivations.

Taylor expansions:

We assume the following Taylor expansions for our functions:

$$\begin{aligned}
u_k(x, t) &= u_k^{(0)}(x, t) + \varepsilon u_k^{(1)}(x, t) + \varepsilon^2 u_k^{(2)}(x, t) + \dots \\
U_k(z, s, t) &= U_k^{(0)}(z, s, t) + \varepsilon U_k^{(1)}(z, s, t) + \varepsilon^2 U_k^{(2)}(z, s, t) + \dots \\
\mu_k(x, t) &= \mu_k^{(0)}(x, t) + \varepsilon \mu_k^{(1)}(x, t) + \varepsilon^2 \mu_k^{(2)}(x, t) + \dots \\
\boldsymbol{\mu}_k(z, s, t) &= \boldsymbol{\mu}_k^{(0)}(z, s, t) + \varepsilon \boldsymbol{\mu}_k^{(1)}(z, s, t) + \varepsilon^2 \boldsymbol{\mu}_k^{(2)}(z, s, t) + \dots \\
\lambda_k(x, t) &= \varepsilon \lambda_k^{(1)}(x, t) + \varepsilon^2 \lambda_k^{(2)}(x, t) + \dots \\
\Lambda_k(z, s, t) &= \varepsilon \Lambda_k^{(1)}(z, s, t) + \varepsilon^2 \Lambda_k^{(2)}(z, s, t) + \dots
\end{aligned}$$

Since the numbering of the phase is present as a subscript, we have put the order in the Taylor expansion as a superscript in brackets. We can then compose these expansions with a regular function F :

$$\begin{aligned}
F(U_k) &= F(U_k^{(0)}) + \varepsilon F'(U_k^{(0)})U_k^{(1)} + \varepsilon^2 \left[F'(U_k^{(0)})U_k^{(2)} + \frac{F''(U_k^{(0)})}{2}(U_k^{(1)})^2 \right] \\
&+ \varepsilon^3 \left[F'(U_k^{(0)})U_k^{(3)} + F''(U_k^{(0)})U_k^{(1)}U_k^{(2)} + \frac{F'''(U_k^{(0)})}{6}(U_k^{(1)})^3 \right] + \dots
\end{aligned}$$

To simplify the notation within the asymptotic, we adopt the following notations for $M(u_k)$

$$M(u_k) = m_k^{(0)} + \varepsilon m_k^{(1)} + \varepsilon^2 m_k^{(2)} + \dots,$$

where each term corresponds to

$$\begin{cases} m_k^{(0)} = M(u_k^{(0)}), \\ m_k^{(1)} = M'(u_k^{(0)})u_k^{(1)}, \\ m_k^{(2)} = M'(u_k^{(0)})u_k^{(2)} + \frac{M''(u_k^{(0)})}{2}(u_k^{(1)})^2. \end{cases}$$

We adopt the same convention for any generic *outer function* $F(u_k)$ or *inner function* $F(U_k)$:

$$\begin{aligned}
F(u_k) &= f_k^{(0)} + \varepsilon f_k^{(1)} + \varepsilon^2 f_k^{(2)} + \varepsilon^3 f_k^{(3)} + \dots \\
F(U_k) &= F_k^{(0)} + \varepsilon F_k^{(1)} + \varepsilon^2 F_k^{(2)} + \varepsilon^3 F_k^{(3)} + \dots
\end{aligned}$$

Flux matching condition between inner and outer equations:

Instead of using the matching conditions directly between the first equations of the inner and outer systems, it is more convenient to perform the matching on the flux

$$j_k = M(u_k) \nabla(\sigma_k \mu_k + \lambda).$$

It has the following Taylor expansion for the model **MCH**

$$\begin{aligned}
(6) \quad j_k &= \left[m_k^{(0)} \nabla(\sigma_k \mu_k^{(0)} + \lambda^{(0)}) \right] + \varepsilon \left[m_k^{(1)} \nabla(\sigma_k \mu_k^{(0)} + \lambda^{(0)}) + m_k^{(0)} \nabla(\sigma_k \mu_k^{(1)} + \lambda^{(1)}) \right] \\
&+ \varepsilon^2 \left[m_k^{(2)} \nabla(\sigma_k \mu_k^{(0)} + \lambda^{(0)}) + m_k^{(1)} \nabla(\sigma_k \mu_k^{(1)} + \lambda^{(1)}) + m_k^{(0)} \nabla(\sigma_k \mu_k^{(2)} + \lambda^{(2)}) \right] + \mathcal{O}(\varepsilon^3).
\end{aligned}$$

In inner coordinates, we only need to express the normal part

$$J_{k,n} := J_k \cdot n = \frac{M(U_k)}{\varepsilon} \partial_z(\sigma_k \boldsymbol{\mu}_k + \Lambda),$$

as the tangential part terms is of higher order. It expands as

$$\begin{aligned}
J_{k,n} = & \frac{1}{\varepsilon} \left[M_k^{(0)} \partial_z (\sigma_k \mu_k^{(0)} + \Lambda^{(0)}) \right], \\
& + \left[M_k^{(1)} \partial_z (\sigma_k \mu_k^{(0)} + \Lambda^{(0)}) + M_k^{(0)} \partial_z (\sigma_k \mu_k^{(1)} + \Lambda^{(1)}) \right], \\
(7) \quad & + \varepsilon \left[M_k^{(2)} \partial_z (\sigma_k \mu_k^{(0)} + \Lambda^{(0)}) + M_k^{(1)} \partial_z (\sigma_k \mu_k^{(1)} + \Lambda^{(1)}) + M_k^{(0)} \partial_z (\sigma_k \mu_k^{(2)} + \Lambda^{(2)}) \right], \\
& + \varepsilon^2 \left[M_k^{(3)} \partial_z (\sigma_k \mu_k^{(0)} + \Lambda^{(0)}) + M_k^{(2)} \partial_z (\sigma_k \mu_k^{(1)} + \Lambda^{(1)}), \right. \\
& \quad \left. + M_k^{(1)} \partial_z (\sigma_k \mu_k^{(2)} + \Lambda^{(2)}) + M_k^{(0)} \partial_z (\sigma_k \mu_k^{(3)} + \Lambda^{(3)}) \right] + \mathcal{O}(\varepsilon^3).
\end{aligned}$$

The flux matching conditions allows to match the limit as $z \rightarrow \pm\infty$ of terms of (6) with the correspond order terms of (7).

We can now investigate order by order the behavior of the models **MCH**. We have to study up to the fourth order term where the leading order of the velocity will appear in the first equation of (5). After that, we adapt the demonstration to the **NMNCH** model, where a reformulation of the problem will be necessary to avoid indeterminate forms in the asymptotic.

2.2. Formal matched asymptotic for multiphasic MCH.

We first establish the Result 1 concerning the properties of the **MCH** model. We recall that we study the behavior of the different terms of the system near the interface Γ_{ij} separating phase i and j . We assume that the following matching conditions for the phase i and j :

$$\begin{aligned}
\lim_{z \rightarrow +\infty} U_i^{(0)} &= 0, & \lim_{z \rightarrow -\infty} U_i^{(0)} &= 1, \\
\lim_{z \rightarrow +\infty} U_i^{(0)} &= 1, & \lim_{z \rightarrow -\infty} U_i^{(0)} &= 0.
\end{aligned}$$

For the other phases, we require the following matching conditions

$$\lim_{z \rightarrow \pm\infty} U_k^{(0)} = 0, \quad \lim_{z \rightarrow \pm\infty} U_k^{(1)} = 0.$$

First order:

At order $(\mathcal{O}(\varepsilon^{-2}), \mathcal{O}(1))$ the inner system reads as

$$\begin{cases} 0 = \partial_z \left(M_k^{(0)} \partial_z (\sigma_k \mu_k^{(0)}) \right), \\ \mu_k^{(0)} = W'(U_k^{(0)}) - \partial_{zz} U_k^{(0)}. \end{cases}$$

From the first equation of the system, we deduce that $M_k^{(0)} \partial_z (\sigma_k \mu_k^{(0)})$ is constant. The matching conditions on the outer (6) and inner fluxes (7) at order ε^{-1} impose this constant to be zero. There is then a constant $A_k^{(0)}$ such that

$$\sigma_k \mu_k^{(0)} = A_k^{(0)}.$$

Collecting all this information, it holds

$$\partial_{zz} U_k^{(0)} - W'(U_k^{(0)}) = \frac{A_k^{(0)}}{\sigma_k} \quad \forall k \in \{1, 2, \dots, L\}.$$

Complemented with the initial conditions

$$\begin{cases} U_i^{(0)} = U_j^{(0)} = \frac{1}{2} \\ U_k^{(0)} = 0 \quad \forall k \in \{1, 2, \dots, L\} \setminus \{i, j\}, \end{cases}$$

Finally, we conclude

$$\begin{cases} U_i^{(0)} = q(z), \\ U_j^{(0)} = q(-z) = 1 - q(z), \\ U_k^{(0)} = 0 \quad \forall k \in \{1, 2, \dots, L\} \setminus \{i, j\}, \\ \mu_k^{(0)} = 0 \quad \forall k \in \{1, 2, \dots, L\}, \end{cases}$$

where q is the optimal phase field profile.

Second order:

At order $(\mathcal{O}(\varepsilon^{-1}), \mathcal{O}(\varepsilon))$ the outer system reads as

$$(8) \quad \begin{cases} 0 = \partial_z \left(M_k^{(0)} \partial_z (\sigma_k \mu_k^{(1)} + \Lambda^{(1)}) \right), \\ \mu_k^{(1)} = W''(U_k^{(0)}) U_k^{(1)} - \partial_{zz} U_k^{(1)} - H_{ij} \partial_z U_k^{(0)}. \end{cases}$$

In particular, it shows that there exists a function $B_k^{(1)}$ constant in z such that

$$M_k^{(0)} \partial_z (\sigma_k \mu_k^{(1)} + \Lambda^{(1)}) = B_k^{(1)}.$$

By matching condition between outer (6) and inner flux (7) at order 1, it holds

$$\lim_{z \rightarrow \pm\infty} M_k^{(0)} \partial_z (\sigma_k \mu_k^{(1)} + \Lambda^{(1)}) = 0.$$

We then deduce that $B_k^{(1)} = 0$ and the existence of a function $A_k^{(1)}$ constant in z such that

$$\sigma_k \mu_k^{(1)} + \Lambda^{(1)} = A_k^{(1)}.$$

Subtracting the case $k = i$ from the case $k = j$ gives

$$\sigma_j \mu_j^{(1)} - \sigma_i \mu_i^{(1)} = A_j^{(1)} - A_i^{(1)}.$$

The term $A_{ij}^{(1)} := A_j^{(1)} - A_i^{(1)}$ can be determined using the second equations of (8). Indeed, recall that

$$\begin{cases} \sigma_i \mu_i^{(1)} = \sigma_i W''(U_i^{(0)}) U_i^{(1)} - \sigma_i \partial_{zz} U_i^{(1)} - \sigma_i H_{ij} q', \\ \sigma_j \mu_j^{(1)} = \sigma_j W''(U_j^{(0)}) U_j^{(1)} - \sigma_j \partial_{zz} U_j^{(1)} + \sigma_j H_{ij} q'. \end{cases}$$

We multiply both equation by q' and integrate the difference. We can eliminate the terms in $U^{(1)}$ through integration by parts:

$$\begin{aligned} \int_{\mathbb{R}} \partial_z (W'(U_i^{(0)})) U_i^{(1)} - \partial_{zz} U_i^{(1)} \partial_z U_i^{(0)} &= \left[W'(U_i^{(0)}) U_i^{(1)} - \partial_z U_i^{(1)} \partial_z U_i^{(0)} \right]_{-\infty}^{+\infty}, \\ &\quad - \int_{\mathbb{R}} \partial_z U_i^{(1)} \left(\underbrace{W'(U_i^{(0)}) - \partial_{zz} U_i^{(0)}}_{=0} \right), \\ &= 0. \end{aligned}$$

It follows that

$$(9) \quad A_{ij}^{(1)} = - \int_{\mathbb{R}} (\sigma_j \mu_j^{(1)} - \sigma_i \mu_i^{(1)}) q' = -(\sigma_j + \sigma_i) H_{ij} \int_{\mathbb{R}} (q')^2 = -\sigma_{ij} c_W H_{ij}.$$

On the other hand, summing the second equation of system (8) for phase i and j gives

$$\mu_i^{(1)} + \mu_j^{(1)} = W''(q) [U_i^{(1)} + U_j^{(1)}] - \partial_{zz} [U_i^{(1)} + U_j^{(1)}].$$

Multiplying by q' and integrating by parts gives:

$$\int_{\mathbb{R}} (\mu_i^{(1)} + \mu_j^{(1)}) q' = 0.$$

This means there exists a profile ζ and a tangential function c such that

$$\mu_i^{(1)} + \mu_j^{(1)} = c(s)\zeta(z).$$

Combining this with equation (9), we obtain

$$\begin{cases} \mu_i^{(1)} = -c_W H_{ij} + \zeta(z)c(s)\frac{\sigma_i}{\sigma_{ij}}, \\ \mu_j^{(1)} = c_W H_{ij} + \zeta(z)c(s)\frac{\sigma_j}{\sigma_{ij}}. \end{cases}$$

and then,

$$\begin{cases} W''(U_i^{(0)})U_i^{(1)} - \partial_{zz}U_i^{(1)} = H_{ij}(c_W + q') + \zeta(z)c(s)\frac{\sigma_i}{\sigma_{ij}}, \\ W''(U_j^{(0)})U_j^{(1)} - \partial_{zz}U_j^{(1)} = -H_{ij}(c_W + q') + \zeta(z)c(s)\frac{\sigma_j}{\sigma_{ij}}. \end{cases}$$

which leads to

$$\begin{cases} U_i^{(1)}(z, s) = H_{ij}\eta(z) + c(s)\frac{\sigma_i}{\sigma_{ij}}\omega(z), \\ U_j^{(1)}(z, s) = -H_{ij}\eta(z) + c(s)\frac{\sigma_j}{\sigma_{ij}}\omega(z). \end{cases}$$

Here η and ω are two profiles respectively defined as the solution of $W'(q)y - y'' = q' + c_W$ and $W'(q)y - y'' = \xi$ with appropriate initial conditions.

In particular, if $H_{ij} \neq 0$, then both $U_i^{(1)}$ and $U_j^{(1)}$ cannot be zero simultaneously which explains why the leading error order term for the solution of the system is ε only. The takeaway is that model **MCH** is always of order 1 when the mean curvature is not null. This result motivates all the interest to use the model **NMCH** which is a second order model.

Third order:

At order $(\mathcal{O}(1), \mathcal{O}(\varepsilon^2))$ the inner system reads as

$$(10) \quad \begin{cases} 0 = \partial_z \left(M_k^{(0)} \partial_z (\sigma_k \mu_k^{(2)} + \Lambda^{(2)}) \right), \\ \mu_k^{(2)} = \frac{W'''(U_k^{(0)})}{2} (U_k^{(1)})^2 + W''(U_k^{(0)})U_k^{(2)} - \partial_{zz}U_k^{(2)} + H_{ij}\partial_z U_k^{(1)} - zH_{ij}^{(2)}\partial_z U_k^{(0)}. \end{cases}$$

In the first equation, we used the results from the first two orders and left out the term that vanish. From the first equality of (10), we find that:

$$M_k^{(0)} \partial_z (\sigma_k \mu_k^{(2)} + \Lambda^{(2)}) = B_k^{(2)}.$$

The matching conditions between the flux (6) and (7) at order ε yields (by removing all the null terms):

$$B_k^{(2)} = \lim_{z \rightarrow \pm\infty} M_k^{(0)} \partial_z (\sigma_k \mu_k^{(2)} + \Lambda^{(2)}) = 0.$$

This means that the term $\sigma_k \mu_k^{(2)} + \Lambda^{(2)}$ is constant in z and will not intervene in the flux term of order ε^2 .

Fourth order:

Collecting the previous results, the first equation of the inner system at order ε for the phase i and j simplifies to

$$\begin{cases} -\frac{1}{\nu_i} V_{ij} q' = \partial_z \left[M_i^{(0)} \partial_z (\sigma_i \mu_i^{(3)} + \Lambda^{(3)}) \right] + \partial_s \left[M_i^{(0)} \partial_s (\sigma_i \mu_i^{(1)} + \Lambda^{(1)}) \right], \\ \frac{1}{\nu_j} V_{ij} q' = \partial_z \left[M_j^{(0)} \partial_z (\sigma_j \mu_j^{(3)} + \Lambda^{(3)}) \right] + \partial_s \left[M_j^{(0)} \partial_s (\sigma_j \mu_j^{(1)} + \Lambda^{(1)}) \right], \end{cases}$$

We subtract the first term equality to the second and integrate. We divide the computation in three:

- The left hand side gives:

$$\left(\frac{1}{\nu_i} + \frac{1}{\nu_j}\right) V_{ij} = \frac{1}{\nu_{ij}} V_{ij}.$$

- Collecting the result from the previous paragraphs, we find the following matching between the outer flux (6) and inner flux (7) at order ε^2 :

$$\lim_{z \rightarrow \pm\infty} M_i^{(0)} \partial_z (\sigma_i \mu_i^{(3)} + \Lambda^{(3)}) = m_i^{(1)} \nabla (\sigma_i \mu_i^{(1)} + \lambda^{(1)}).$$

Because $M'(0) = M'(1) = 0$, the limit term is zero and then

$$\int_{\mathbb{R}} \partial_z \left(M_i^{(0)} \partial_z (\sigma_i \mu_i^{(3)} + \Lambda^{(3)}) \right) = 0.$$

The integral of the j -th phase is treated similarly.

- Using (9), the second term of the right hand side is (noting that $M_i^{(0)} = M_j^{(0)}$):

$$\int_{\mathbb{R}} M_i^{(0)} \partial_{ss} (\sigma_i \mu_i^{(1)} - \sigma_j \mu_j^{(1)}) = \sigma_{ij} \left(\int_{\mathbb{R}} M(q(z)) dz \right) c_W \partial_{ss} H_{ij}.$$

Finally, we observe that

$$\frac{1}{\nu_{ij}} V_{ij} = \sigma_{ij} c_W c_M \partial_{ss} H_{ij}.$$

2.3. Formal matched asymptotic for the multiphase NMNCH model. We demonstrate Result 2 concerning the properties of **NMNCH**. We assume the following matching conditions for the phase i and j ,

$$\begin{aligned} \lim_{z \rightarrow +\infty} U_i^{(0)} &= 0, & \lim_{z \rightarrow -\infty} U_i^{(0)} &= 1, \\ \lim_{z \rightarrow +\infty} U_i^{(0)} &= 1, & \lim_{z \rightarrow -\infty} U_i^{(0)} &= 0, \end{aligned}$$

and for the other phases

$$\lim_{z \rightarrow \pm\infty} U_k^{(0)} = 0, \quad \lim_{z \rightarrow \pm\infty} U_k^{(1)} = 0.$$

Reformulation of the model:

It is more appropriate to rewrite the model **NMNCH** by transferring the $N(u_k)$ in the left hand sides of the system:

$$(11) \quad \begin{cases} \varepsilon^2 g(u_k) \partial_t u_k = \nu_k \operatorname{div} (M(u_k) \nabla (\sigma_k \mu_k + \lambda)), \\ g(u_k) \mu_k = W'(u_k) - \varepsilon^2 \Delta u_k. \end{cases}$$

where $g(u_k) = \frac{1}{N(u_k)} = \sqrt{M(u_k)}$. The advantage of such a formulation is that $g(u_k)$ is always well defined even if $u_k = 0$, which is not the case for $N(u_k)$. Note also that μ_k has been changed but we kept the same notation.

The inner system now reads:

$$\left\{ \begin{aligned} & \frac{\varepsilon^2 G_k}{\nu_k} \partial_t U_k + \frac{\varepsilon^2 G_k}{\nu_k} \partial_t S \partial_s U_k - \frac{\varepsilon G_k}{\nu_k} V_{ij} \partial_z U_k = \frac{1}{\varepsilon^2} \partial_z (M_k \partial_z (\sigma_k \mu_k + \Lambda)) \\ & \quad + \frac{M_k}{\varepsilon} \Delta d_{ij} \partial_z (\sigma_k \mu_k + \Lambda) + T_1(s), \\ & G_k \mu_k = W'(U_k) - \partial_{zz} U_k - \varepsilon \Delta d_{ij} \partial_z U_k + \varepsilon^2 T_2(s), \\ & \Delta d_{ij} = \frac{H_{ij}}{1 + \varepsilon z H_{ij}} = H_{ij} - \varepsilon z H_{ij}^2 + \mathcal{O}(\varepsilon^2), \\ & T_1(s) = \frac{1}{(1 + \varepsilon z H_{ij})^2} \partial_s (M_k \partial_s (\sigma_k \mu_k + \Lambda)) - \frac{\varepsilon z M_k \partial_s H_{ij}}{(1 + \varepsilon z H_{ij})^3} \partial_s (\sigma_k \mu_k + \Lambda), \\ & T_2(s) = \frac{1}{(1 + \varepsilon z H_{ij})^2} \partial_{ss} U_k - \frac{\varepsilon z \partial_s H_{ij}}{(1 + \varepsilon z H_{ij})^3} \partial_s U_k. \end{aligned} \right.$$

Because the $N(u_k)$ are now on the left hand side of the system in the form of G_k , the flux term $j = M(u_k)\nabla(\sigma_k\mu_k + \lambda_k)$ is the same as the one for **MCH**. The flux matching condition is then also equal to the one given by (6) and (7).

First order:

At order $(\mathcal{O}(\varepsilon^{-2}), \mathcal{O}(1))$ the inner system reads:

$$\begin{cases} 0 = \partial_z \left(M_k^{(0)} \partial_z (\sigma_k \mu_k^{(0)}) \right), \\ G_k^{(0)} \mu_k^{(0)} = W'(U_k^{(0)}) - \partial_{zz} U_k^{(0)}. \end{cases}$$

From the first equation of the system, we deduce that $M_k^{(0)} \partial_z (\sigma_k \mu_k^{(0)})$ is constant. The matching conditions on the outer (6) and inner fluxes (7) at order ε^{-1} impose this constant to be zero. Then there exists a constant $A_k^{(0)}$ in z such that

$$\sigma_k \mu_k^{(0)} = A_k^{(0)}.$$

Collecting all this information, we have

$$\partial_{zz} U_k^{(0)} - W'(U_k^{(0)}) = \frac{G(U_k^{(0)}) A_k^{(0)}}{\sigma_k}, \quad \forall k \in \{1, \dots, L\}.$$

Then, using the matching conditions and the initial conditions $U_i^{(0)} = U_j^{(0)} = \frac{1}{2}$ lead to

$$\begin{cases} U_i^{(0)} = q(z), \\ \mu_i^{(0)} = 0, \\ U_j^{(0)} = q(-z) = 1 - q(z), \\ \mu_j^{(0)} = 0, \\ U_k^{(0)} = 0 \quad \forall k \in \{1, \dots, L\} \setminus \{i, j\}. \end{cases}$$

Notice that $\mu_k^{(0)}$ is a constant in z that can be nonzero.

Second order:

At order $(\mathcal{O}(\varepsilon^{-1}), \mathcal{O}(\varepsilon))$ the inner system reads

$$(12) \quad \begin{cases} 0 = \partial_z \left(M_k^{(0)} \partial_z (\sigma_k \mu_k^{(1)} + \Lambda^{(1)}) \right), \\ G_k^{(0)} \mu_k^{(1)} + G_k^{(1)} \mu_k^{(0)} = W''(U_k^{(0)}) U_k^{(1)} - \partial_{zz} U_k^{(1)} - H_{ij} \partial_z U_k^{(0)}. \end{cases}$$

For $k \neq i, j$, using the fact that $U_k^{(0)} = 0$, the second equation can be rewritten as

$$0 = \left(1 - \mu_k^{(0)} \right) U_k^{(1)} - \partial_{zz} U_k^{(1)}.$$

As the matching conditions shows that $\lim_{z \rightarrow \pm\infty} U_k^{(1)} = 0$, it follows that $U_k^{(1)} = 0$.

Now turning to the i -th phase (resp j -th), there exists a function $B_i^{(1)}$ constant in z such that

$$M_i^{(0)} \partial_z (\sigma_i \mu_i^{(1)} + \Lambda^{(1)}) = B_i^{(1)}.$$

By matching condition between outer (6) and inner flux (7) at order 1, we have

$$\lim_{z \rightarrow \pm\infty} M_i^{(0)} \partial_z (\sigma_i \mu_i^{(1)} + \Lambda^{(1)}) = 0,$$

and $B_i^{(1)} = 0$ (resp $B_j^{(1)} = 0$). There then exists functions $A_i^{(1)}, A_j^{(1)}$ constant in z such that

$$\begin{cases} \sigma_i \mu_i^{(1)} + \Lambda^{(1)} = A_i^{(1)}, \\ \sigma_j \mu_j^{(1)} + \Lambda^{(1)} = A_j^{(1)}. \end{cases}$$

Subtracting the i -th term to the j -th term conduces to

$$\sigma_j \mu_j^{(1)} - \sigma_i \mu_i^{(1)} = A_j^{(1)} - A_i^{(1)} := A_{ij}^{(1)}.$$

Moreover, recall that $U_k^{(1)} = 0$ for $k \neq i, j$, which imply that $U_i^{(1)} = -U_j^{(1)}$ as $\sum_{k=1}^N U_k^{(1)} = 0$. Using the symmetry properties $g(1-s) = g(s)$ and $W''(1-s) = W''(s)$, it follows

$$\begin{aligned} g(U_j^{(0)}) \mu_j^{(1)} &= W''(U_j^{(0)}) U_j^{(1)} - \partial_{zz} U_j^{(1)} - H_{ij} \partial_z U_j^{(0)}, \\ &= -W''(U_i^{(0)}) U_i^{(1)} + \partial_{zz} U_i^{(1)} + H_{ij} \partial_z U_i^{(0)}, \\ &= -g(U_i^{(0)}) \mu_i^{(1)}, \\ &= -g(U_j^{(0)}) \mu_i^{(1)}. \end{aligned}$$

and then $g(U_j^{(0)}) (\mu_i^{(1)} + \mu_j^{(1)}) = 0$. Finally, as $g(q) \neq 0$, necessarily $\mu_i^{(1)}$ and $\mu_j^{(1)}$ are constant in z and

$$\mu_j^{(1)} = -\mu_i^{(1)}.$$

It shows that we can express $A_{ij}^{(1)}$ as

$$A_{ij}^{(1)} = (\sigma_j + \sigma_i) \mu_j^{(1)} = -\sigma_{ij} \mu_i^{(1)}.$$

Now, multiplying the second equation of (12) for phase i

$$g(U_i^{(0)}) \mu_i^{(1)} = W''(U_i^{(0)}) U_i^{(1)} - \partial_{zz} U_i^{(1)} - H_{ij} q',$$

by the profile q' and integrating over \mathbb{R} show that

$$(13) \quad \mu_i^{(1)} = -\frac{c_W}{c_N} H_{ij} \quad \text{and} \quad A_{ij}^{(1)} = \frac{c_W}{c_N} \sigma_{ij} H_{ij}.$$

Indeed, on the one hand we have

$$\begin{aligned} \int_{\mathbb{R}} \partial_z (W'(U_i^{(0)})) U_i^{(1)} - \partial_{zz} U_i^{(1)} \partial_z U_i^{(0)} &= [W'(U_i^{(0)}) U_i^{(1)} - \partial_z U_i^{(1)} \partial_z U_i^{(0)}]_{-\infty}^{+\infty}, \\ &\quad - \int_{\mathbb{R}} \partial_z U_i^{(1)} \left(\underbrace{W'(U_i^{(0)}) - \partial_{zz} U_i^{(0)}}_{=0} \right), \\ &= 0, \end{aligned}$$

and on the other side

$$\int_{\mathbb{R}} g(q) \mu_i^{(1)} q' = \mu_i^{(1)} \int_{\mathbb{R}} \frac{q'}{N(q)} = c_N \mu_i^{(1)}, \quad \text{and} \quad \int_{\mathbb{R}} H_{ij} (q')^2 = c_W H_{ij}.$$

Finally, it shows that

$$\partial_{zz} U_i^{(1)} - W''(q) U_i^{(1)} = -H_{ij} (q' - \frac{c_W}{c_N} g(q)).$$

Now, recall that the choice to use the mobilities $M(s) = \sqrt{2W(s)}$ and $N(s) = 1/\sqrt{M(s)} = 1/\sqrt{2W(s)}$ implies that

$$g(q) = 1/N(q) = \sqrt{2W(q)} = -q' \quad \text{and} \quad c_N = -c_W.$$

This is the key point to understand why in this case the term $U_i^{(1)}$ is null as a solution of

$$\partial_{zz} U_i^{(1)} - W''(q) U_i^{(1)} = 0.$$

The same argument gives $U_j^{(1)} = 0$. In summary, we have $U_k^{(1)} = U_i^{(1)} = U_j^{(1)} = 0$. It means that the leading error order term in the solutions U_i and U_j is of magnitude ε^2 while the other phases are absent.

Third order:

Using the two previous order, at order $(\mathcal{O}(1), \mathcal{O}(\varepsilon^2))$, the inner system simplifies to

$$\begin{cases} 0 = \partial_z \left(M_k^{(0)} \partial_z (\sigma_k \mu_k^{(2)} + \Lambda^{(2)}) \right), \\ G_k^{(0)} \mu_k^{(2)} = \frac{W'''(U_k^{(0)})}{2} (U_k^{(1)})^2 + W''(U_k^{(0)}) U_k^{(2)} - \partial_{zz} U_k^{(2)} + H_{ij} \partial_z U_k^{(1)} - z H_{ij}^2 \partial_z U_k^{(2)}. \end{cases}$$

From the first equality, we find that

$$M_k^{(0)} \partial_z (\sigma_k \mu_k^{(2)} + \Lambda^{(2)}) = B_2.$$

The matching conditions between the flux (6) and (7) at order ε yields (by removing all the null terms) gives also

$$B_2 = \lim_{z \rightarrow \pm\infty} M_k^{(0)} \partial_z (\sigma_k \mu_k^{(2)} + \Lambda^{(2)}) = 0.$$

This means that $\sigma_k \mu_k^{(2)} + \Lambda^{(2)}$ is constant in z and will not intervene in the flux term of order ε^2 .

Remark 2.1. *It possible to show that $U_i^{(2)}$ and $U_j^{(2)}$ are of the form*

$$U_j^{(2)} = -U_i^{(2)} = H_{ij}^2 \zeta(z),$$

where ζ is the profile defined by

$$\begin{cases} y''(z) - W''(q)y(z) = zq' \\ y(0) = 0 \end{cases}$$

and decreases to zero at infinity.

Fourth order:

Eliminating all the vanishing terms, the first equations for the i -th and j -th phase of the inner system read

$$(14) \quad \begin{aligned} -\frac{1}{\nu_i} V_{ij} g(U_i^{(0)}) \partial_z U_i^{(0)} &= \partial_z \left[M_i^{(0)} \partial_z (\sigma_i \mu_i^{(3)} + \Lambda^{(3)}) \right] + \partial_s \left[M(U_i^{(0)}) \partial_s (\sigma_i \mu_i^{(1)} + \Lambda^{(1)}) \right], \\ -\frac{1}{\nu_j} V_{ij} g(U_j^{(0)}) \partial_z U_j^{(0)} &= \partial_z \left[M_j^{(0)} \partial_z (\sigma_j \mu_j^{(3)} + \Lambda^{(3)}) \right] + \partial_s \left[M(U_j^{(0)}) \partial_s (\sigma_j \mu_j^{(1)} + \Lambda^{(1)}) \right]. \end{aligned}$$

Integrating over \mathbb{R} yields to

$$\begin{aligned} -\frac{c_N}{\nu_i} V_{ij} &= \int_{\mathbb{R}} \partial_z \left[M(U_i^{(0)}) \partial_z (\sigma_i \mu_i^{(3)} + \Lambda^{(3)}) \right] + \int_{\mathbb{R}} \partial_s \left[M(U_i^{(0)}) q' \partial_s (\sigma_i \mu_i^{(1)} + \Lambda^{(1)}) \right], \\ +\frac{c_N}{\nu_j} V_{ij} &= \int_{\mathbb{R}} \partial_z \left[M(U_j^{(0)}) \partial_z (\sigma_j \mu_j^{(3)} + \Lambda^{(3)}) \right] + \int_{\mathbb{R}} \partial_s \left[M(U_j^{(0)}) q' \partial_s (\sigma_j \mu_j^{(1)} + \Lambda^{(1)}) \right]. \end{aligned}$$

The matching conditions on the fluxes at order $\mathcal{O}(\varepsilon^2)$ shows that the first integral is zero. Note that most of the terms in the fluxes have been proven to be zero in the previous orders.

On the other hand, the second integral can be expressed with the terms from the second order calculations and the properties of the profile q give that

$$\begin{aligned} \int_{\mathbb{R}} \partial_s \left[M(U_i^{(0)}) \partial_s (\sigma_i \mu_i^{(1)} + \Lambda^{(1)}) \right] &= \partial_{ss} (\sigma_i \mu_i^{(1)} + \Lambda^{(1)}) \int_{\mathbb{R}} M(q), \\ &= c_M \partial_{ss} (\sigma_i \mu_i^{(1)} + \Lambda^{(1)}). \end{aligned}$$

The same result can be obtained for the integral in j . Subtracting the first equation of (14) to the second, we get

$$\frac{1}{\nu_{ij}} c_N V_{ij} = \left(\frac{1}{\nu_i} + \frac{1}{\nu_j} \right) c_N V_{ij} = c_M \partial_{ss} \left(-\sigma_i^{(1)} \mu_i^{(1)} - \Lambda^{(1)} + \sigma_j \mu_j^{(1)} + \Lambda^{(1)} \right) = c_M \partial_{ss} A_{ij}^{(1)}.$$

Using (13), it follows that

$$\frac{1}{\nu_{ij}} V_{ij} = \frac{c_W c_M}{(c_N)^2} \sigma_{ij} \partial_{ss} H_{ij},$$

which concludes the proof of Result 2.

3. NUMERICAL SECTION(S)

In this section, we explain how to efficiently compute the solutions of the phase field models **MCH** and **NMNCH** and give some various numerical illustrations of these models in 2 and 3 dimensions. Recall that these models read as follows:

- **MCH** model

$$\begin{cases} \partial_t u_k &= \nu_k \operatorname{div} (M(u_k) \nabla (\sigma_k \mu_k + \lambda)) \\ \mu_k &= \frac{W'(u_k)}{\varepsilon^2} - \Delta u_k \\ 1 &= \sum_k u_k \end{cases}$$

where the mobility M is defined as $M(u) = \frac{1}{c_N^2} 2W(u)$. Here, the constant $|c_N| = \frac{1}{6}$ is added to get the same limit law as using our new Cahn–Hilliard model.

- **NMNCH** model

$$\begin{cases} \partial_t u_k &= \nu_k N(u_k) \operatorname{div} (M(u_k) \nabla N(u_k) (\sigma_k \mu_k + \lambda)) \\ \mu_k &= \frac{W'(u_k)}{\varepsilon^2} - \Delta u_k \\ 1 &= \sum_k u_k \end{cases}$$

where the mobilities M and N are defined by $M(u) = 2W(u) + \gamma \varepsilon^2$ and $N(u) = \frac{1}{\sqrt{M(u)}}$. Here $\gamma > 0$ is a smoothing parameter and we take $\gamma = 1$ for all numerical experiments presented below.

Remark 3.1. *The addition of the term $\gamma \varepsilon^2$ in the mobility does not change the asymptotic results, at least the first four orders of interests. Indeed, this term will be associated with μ_0 that is zero and μ_1 whose derivative in z vanishes. Also, as the mobility M is never zero, the term $N(u) = \frac{1}{\sqrt{M(u)}}$ doesn't get infinite and no further precaution is required.*

Various schemes have already been proposed in the literature [75, 49, 46, 47] to deal with multiphasic Cahn–Hilliard type equations, especially when $L = 3$ [7, 11, 39, 40, 42, 26, 9] and $L = 4$ [41, 43, 77, 47].

About the Cahn Hilliard equation, recall that the system is of fourth-order in space, which introduces severe restrictions on the time step for most classical methods due to numerical instability. To overcome these difficulties, an natural idea is to adapt the convex splitting strategy of the Cahn–Hilliard energy, which was first proposed by Eyre [35] and became popular as a simple, efficient, and stable scheme to approximate various evolution problems with a gradient flow structure [25, 73, 36, 33, 65, 66, 31]. For instance, a first- and second-order splitting scheme was proposed in [6, 62, 61] to address the case of the Cahn–Hilliard equation with mobility. However, these approaches are based on the finite element method and requires the resolution of linear system at each step which can be ill-conditioned in the case of degenerated mobilities. In this direction, we recently propose in [17] a semi-implicit Fourier spectral method in the spirit of [23, 13, 15, 18, 14]. Here, the idea is to exploit the variational structure of the mobility

by using an additionally convex splitting of its associated metric. In such way, we obtain a very simple, efficient and stable scheme even in the case of degenerated mobilities.

About the system of Cahn Hilliard equations, recall that in [47], the authors propose a accurate non linear multigrid method. However, this approach requires the resolution of an $2L \times 2L$ system of equations which can be problematic when L is large. Based on the first-order convex splitting method, Lee and al [46] developed a practically unconditionally gradient stable conservative nonlinear numerical scheme for converting the L -phase Cahn-Hilliard system into a system of L Cahn-Hilliard equations. This reduces significantly the computational cost. More recently, Yang and Kim [75] proposed an unconditionally stable with second-order accuracy based on the Crank-Nicolson scheme and adopt the idea of stabilized method [78].

In this paper, we propose to adapt our approach proposed in [17] for the multiphase context. The novelty is to split the treatment of the Lagrange multiplier via the splitting of the metric such as **MCH** and **NMNCH** can be solved in a decoupled way. This means that we only need to solve L biphasic Cahn-Hilliard equations at each iteration, as in [46].

In this section, we first recall the schemes we have introduced in [17] when only one phase is considered for both models **MCH** and **NMNCH**. We then extend to the multiphase case by using a semi-implicit treatment of the Lagrange multiplier which is explicitly given in Fourier space. For each model, a **Matlab** script is provided to give an example of implementation. Secondly, we propose a numerical comparison of phase field models in space dimension 2. In addition, some illustrations are provided to show the influence of mobilities and surface tensions using the model **NMNCH**. These illustrations also show that our models can handle with Cahn-Hilliard problems in complex domain without imposing any boundary condition or adding surface energy. This simply requires imposing null mobility at the appropriate interfaces. We then conclude this section with an application to wetting problem where we derive a simplified model using the liquid phase only.

3.1. Spatial and time discretization: a Fourier-spectral approach. All equations are solved on a square-box $Q = [0, L_1] \times \dots \times [0, L_d]$ with periodic boundary conditions. We recall that the Fourier \mathbf{K} -approximation of a function u defined in a box $Q = [0, L_1] \times \dots \times [0, L_d]$ is given by

$$u^K(x) = \sum_{\mathbf{k} \in K_N} c_{\mathbf{k}} e^{2i\pi \boldsymbol{\xi}_{\mathbf{k}} \cdot x},$$

where $K_N = [-\frac{N_1}{2}, \frac{N_1}{2} - 1] \times \dots \times [-\frac{N_d}{2}, \frac{N_d}{2} - 1]$, $\mathbf{k} = (k_1, \dots, k_d)$ and $\boldsymbol{\xi}_{\mathbf{k}} = (k_1/L_1, \dots, k_d/L_d)$. In this formula, the $c_{\mathbf{k}}$'s denote the K^d first discrete Fourier coefficients of u . The inverse discrete Fourier transform leads to $u_{\mathbf{k}}^K = \text{IFFT}[c_{\mathbf{k}}]$ where $u_{\mathbf{k}}^K$ denotes the value of u at the points $x_{\mathbf{k}} = (k_1 h_1, \dots, k_d h_d)$ and where $h_i = L_i/N_i$ for $i \in \{1, \dots, d\}$. Conversely, $c_{\mathbf{k}}$ can be computed as the discrete Fourier transform of $u_{\mathbf{k}}^K$, i.e., $c_{\mathbf{k}} = \text{FFT}[u_{\mathbf{k}}^K]$.

Given a time discretization parameter $\delta_t > 0$, we construct a sequence $(u^n)_{n \geq 0}$ of approximations of u at times $n\delta_t$.

3.2. Numerical scheme for model MCH. We first recall here the numerical approach introduced in [17] to compute numerical solutions of the **MCH** model in the one phase context. In such case, the Cahn Hilliard equation reads as

$$\begin{cases} \partial_t u_k &= \text{div}(M(u_k) \nabla(\mu_k)), \\ \mu_k &= \frac{W'(u_k)}{\varepsilon^2} - \Delta u_k. \end{cases}$$

Our approach can be viewed as a Fourier-semi implicit scheme which reads as

$$\begin{cases} (u^{n+1} - u^n)/\delta_t &= m \Delta \mu^{n+1} + \text{div}((M(u^n) - m) \nabla \mu^n) \\ \mu^{n+1} &= \left(-\Delta u^{n+1} + \frac{\alpha}{\varepsilon^2} u^{n+1}\right) + \left(\frac{1}{\varepsilon^2} (W'(u^n) - \alpha u^n)\right). \end{cases}$$

where m and α are two stabilized parameters. More precisely, this scheme derive from a convex-concave splitting of the Cahn Hilliard energy

$$\int_Q \varepsilon \frac{|\nabla u|^2}{2} + \frac{1}{\varepsilon} W(u) dx = \frac{1}{2} \int_Q \varepsilon |\nabla u|^2 + \frac{\alpha}{\varepsilon^2} u^2 dx + \int_Q \frac{1}{\varepsilon} (W(u) - \alpha \frac{u^2}{2}) dx,$$

but also for the associated metric

$$\frac{1}{2} \int_Q M(u^n) |\nabla \mu|^2 dx = \frac{1}{2} \int_Q m |\nabla \mu|^2 dx + \frac{1}{2} \int_Q (M(u^n) - m) |\nabla \mu|^2 dx.$$

As we explained in [17], the scheme seems to decrease the Cahn Hilliard energy as soon as each explicit term is concave which is true using $m = \max_{s \in [0,1]} \{M(s)\}$ and $\alpha \geq \max_{s \in [0,1]} |W''(s)|$.

Alternatively this scheme reads in a matrix form as

$$\begin{pmatrix} I_d & -\delta_t m \Delta \\ \Delta - \alpha/\varepsilon^2 & I_d \end{pmatrix} \begin{pmatrix} u^{n+1} \\ \mu^{n+1} \end{pmatrix} = \begin{pmatrix} B_{u^n, \mu^n}^1 \\ B_{u^n, \mu^n}^2 \end{pmatrix},$$

where

$$\begin{pmatrix} B_{u^n, \mu^n}^1 \\ B_{u^n, \mu^n}^2 \end{pmatrix} = \begin{pmatrix} u^n + \delta_t \operatorname{div}((M(u^n) - m) \nabla \mu^n) \\ \frac{1}{\varepsilon^2} (W'(u^n) - \alpha u^n) \end{pmatrix}.$$

Finally, the couple (u^{n+1}, μ^{n+1}) can be computed using the system

$$\begin{cases} u^{n+1} &= L_M \left[B_{u^n, \mu^n}^1 + \delta_t m \Delta B_{u^n, \mu^n}^2 \right], \\ \mu^{n+1} &= L_M \left[(-\Delta B_{u^n, \mu^n}^1 + \alpha/\varepsilon^2 B_{u^n, \mu^n}^1) + B_{u^n, \mu^n}^2 \right], \end{cases}$$

where the operator L_M is given by

$$L_M = \left(I_d + \delta_t m \Delta (\Delta - \alpha/\varepsilon^2 I_d) \right)^{-1},$$

and can be computed efficiently in Fourier space.

Remark 3.2. *This scheme is very efficient as it does not require some resolution of linear system. Moreover, this scheme seems to be stable without assumption on δ_t in the sense that it decreases the Cahn Hillard energy. It is also not difficult to show that the mass of u is conserved along the iteration*

$$\int_Q u^{n+1} dx = \int_Q u^n dx.$$

Following this method, we now propose similar schemes for the multiphase **MCH** model

$$\begin{cases} \partial_t u_k &= \nu_k \operatorname{div} (M(u_k) \nabla (\sigma_k \mu_k + \lambda)), \\ \mu_k &= \frac{W'(u_k)}{\varepsilon^2} - \Delta u_k, \\ 1 &= \sum_k u_k. \end{cases}$$

They are based on the same convex-concave splitting of the Cahn-Hillard equation and its associated metric. In the multiphase context, it reads as

$$\begin{cases} (u_k^{n+1} - u_k^n)/\delta_t &= \nu_k \left(m \Delta [\sigma_k \mu_k^{n+1} + \lambda^{n+1}] + \operatorname{div} [(M(u_k^n) - m) \nabla [\sigma_k \mu_k^n + \lambda^n]] \right), \\ \mu_k^{n+1} &= \left(-\Delta u_k^{n+1} + \frac{\alpha}{\varepsilon^2} u_k^{n+1} \right) + \left(\frac{1}{\varepsilon^2} (W'(u_k^n) - \alpha u_k^n) \right), \end{cases}$$

where the Lagrange multiplier λ^{n+1} is defined to satisfy the partition constraint $\sum_k u_k^{n+1} = 1$.

More precisely, the couple (u_k^{n+1}, μ_k^{n+1}) can be expressed as

$$\begin{cases} u_k^{n+1} &= u_k^{n+1/2} + \delta_t \nu_k m L_{M_k} [\Delta \lambda^{n+1}], \\ \mu_k^{n+1} &= \mu_k^{n+1/2} + \delta_t \nu_k m L_{M_k} \left[\left(-\Delta + \frac{\alpha}{\varepsilon^2} \right) \Delta \lambda^{n+1} \right], \end{cases}$$

where

- the operator L_{M_k} is given by

$$L_{M_k} = \left(I_d + \delta_t m \sigma_k \nu_k \Delta (\Delta - \alpha/\varepsilon^2 I_d) \right)^{-1}.$$

- the couple $(u_k^{n+1/2}, \mu_k^{n+1/2})$ are defined as the solution of the decoupled system

$$\begin{cases} u_k^{n+1/2} &= L_{M_k} \left[B_{u_k^n, \mu_k^n}^1 + \delta_t m \sigma_k \nu_k \Delta B_{u_k^n, \mu_k^n}^2 \right], \\ \mu_k^{n+1/2} &= L_{M_k} \left[(-\Delta + \alpha/\varepsilon^2) B_{u_k^n, \mu_k^n}^1 + B_{u_k^n, \mu_k^n}^2 \right], \end{cases}$$

where

$$B_{u_k^n, \mu_k^n}^1 = u_k^n + \delta_t \nu_k \operatorname{div} \left[(M(u_k^n) - m) \nabla [\sigma_k \mu_k^n + \lambda^k] \right],$$

and

$$B_{u_k^n, \mu_k^n}^2 = \frac{1}{\varepsilon^2} (W'(u_k^n) - \alpha u_k^n).$$

In particular, it shows that λ^{n+1} satisfies the following equation

$$\delta_t m \left(\sum_k \nu_k L_{M_k} \right) \Delta \lambda^{n+1} = 1 - \sum_k u_k^{n+1/2},$$

and then

$$\lambda^{n+1} = \frac{1}{\delta_t m} \left[\sum_k \nu_k L_{M_k} \Delta \right]^{-1} \left(1 - \sum_k u_k^{n+1/2} \right).$$

Here the operator $[\sum_k \nu_k L_{M_k} \Delta]^{-1}$ is still homogeneous and can be computed easily in Fourier space.

From the previous equations, we can implement the schemes within the **Matlab** framework almost immediately. Indeed as showcased in Figure (1), we can write a **Matlab** script approximating the solution of model **MCH** with less than 60 lines. In particular :

- We consider here a discretized computation box $Q = [-1/2, 1/2]^2$ using $N = 2^8$ nodes in each direction. The initial condition of u is an uniform noise and the numerical parameters are given by $\varepsilon = 1/N$, $\delta_t = \varepsilon^4$, $\alpha = 2$, and $m = \max_{s \in [0,1]} M(s)$.
- First we define the terms $u_k^{n+1/2}$ and $\mu_k^{n+1/2}$ (lines 29-39) as in [17]. Then, we determine λ^{n+1} (lines 42-45) which allows us to correct and obtain u_k^{n+1} and μ_k^{n+1} (lines 48-52).
- Line 24 corresponds to the definition of the Fourier-symbol associated with operator L_{M_k} . The application of L_{M_k} can then be performed by using a simple multiplication in Fourier space with the array M_L .
- Each computation of gradient and divergence operator are made in Fourier space. For instance the divergence $\operatorname{div} \left[(M(u_k^n) - m) \nabla [\sigma_k \mu_k^n + \lambda^k] \right]$ is computed on the line 31.
- The computation of λ^{n+1} is illustrated from line 42 to 45. λ^{n+1} is first computed in Fourier space using the Fourier-symbol of the operator $[\sum_k \nu_k L_{M_k} \Delta]^{-1}$. Then λ^{n+1} is obtained by applying the discrete inverse Fourier transform.

3.3. Numerical scheme of the NMNCH phase field model. The case of the **NM-NCH** phase field model is slightly more complicated and we first recall the numerical scheme introduced in [17] for only one phase and we then explain how to generalize it in the multiphase context. Recall that model **NMNCH** reads as

$$\begin{cases} \partial_t u_k &= N(u_k) \operatorname{div} (M(u_k) \nabla (N(u_k) \mu_k)) \\ \mu_k &= \frac{W'(u_k)}{\varepsilon^2} - \Delta u_k \end{cases}$$

and that our Fourier semi-implicit scheme in the biphasic case reads as

$$\begin{cases} (u^{n+1} - u^n)/\delta_t &= [m\Delta - \beta] \mu^{n+1} + H(u^n, \mu^n), \\ \mu^{n+1} &= \left(-\Delta u^{n+1} + \frac{\alpha}{\varepsilon^2} u^{n+1} \right) + \left(\frac{1}{\varepsilon^2} (W'(u^n) - \alpha u^n) \right), \end{cases}$$

```

1 clear all; colormap('jet');
2
3 %%%%%%%%%%% parameters %%%%%%%%%%%
4 N = 2^8; epsilon =1/N; dt = epsilon^4; T = 10^(-4);
5 W_prim = @(U) (U.*(U-1).*(2*U-1));
6 MobMM = @(U) 2*36/2*(((U).*(1-U)).^2) );
7 alpha = 2;x = linspace(0,1,N); c=max(MobMM(x));
8 %%%%%%%%%%% condition initiale %%%%%%%%%%%
9 U(:,:,1) = 2*rand(N,N)/3; U(:,:,2) = rand(N,N).*(1 -U(:,:,1) );
10 U(:,:,3) = 1-(U(:,:,1) + U(:,:,2) );
11 Mu = 0*U;lambda = 0; lambda_fourier = 0;Mu_fourier = zeros(N,N,3);
12 for k=1:3, U_fourier(:,:,k) = fft2(U(:,:,k)); end
13
14 %%%%%%%%%%% coefficient - mobilite %%%%%%%%%%%
15 sigma12 =1; sigma13 =1; sigma23 =1;
16 sigma(1) = (sigma12 + sigma13 - sigma23)/2;
17 sigma(2) = (sigma12 + sigma23 - sigma13)/2;
18 sigma(3) = (sigma23 + sigma13 - sigma12)/2;
19 mob(1) = 1; mob(2)= 1; mob(3) = 1;
20 %%%%%%%%%%% Diffusion Fourier %%%%%%%%%%%
21 k = [0:N/2,-N/2+1:-1];
22 [K1,K2] = meshgrid(k,k);
23 Delta = -4*pi^2*((K1.^2 + (K2).^2));
24 for k=1:3, M_L(:,:,k) = 1./(1 + dt*sigma(k)*mob(k)*(c*Delta).*(Delta - alpha/epsilon
    ^2)); end
25 %%%%%%%%%%%
26 k=1;
27 for i=1:T/dt,
28 %%%%%%%%%%% computation of u^{n+1/2}_k, \mu^{n+1/2}_k
29 for k=1:3,
30 mobUk = MobMM(U(:,:,k));
31 div_mob_laplacien_fourier = 2*1i*pi*K1.*fft2((mobUk-c).*(fft2(2*1i*pi*K1.*(sigma(k)*
    Mu_fourier(:,:,k) + lambda_fourier))))...
32 + 2*1i*pi*K2.*fft2((mobUk-c).*(fft2(2*1i*pi*K2.*(sigma(k)*Mu_fourier(:,:,k) +
    lambda_fourier))));
33 B1 = U_fourier(:,:,k) + dt*mob(k)*div_mob_laplacien_fourier;
34 B2 = fft2(W_prim(U(:,:,k))/epsilon^2 - alpha/epsilon^2*U(:,:,k));
35 U_fourier(:,:,k) = M_L(:,:,k).*(B1 + dt*mob(k)*sigma(k)*c*Delta.*B2);
36 U(:,:,k) = real(ifft2(U_fourier(:,:,k)));
37 Mu_fourier(:,:,k) = M_L(:,:,k).*((alpha/epsilon^2 - Delta).*B1 + B2);
38 Mu(:,:,k) = ifft2(Mu_fourier(:,:,k));
39 end
40
41 %%%%%%%%%%% computation of lambda and correction %%%%%%%%%%%
42 Err_sum = fft2(1 - sum(U,3));
43 lambda_fourier = (1./((c*(M_L(:,:,1)*mob(1) +M_L(:,:,2)*mob(2) + M_L(:,:,3)*mob(3))).*
    Delta)).*Err_sum/dt;
44 lambda_fourier(1,1) = 0;
45 lambda = real(ifft2(lambda_fourier));
46
47 for k=1:3,
48 term = dt*(mob(k)*(c*Delta.*lambda_fourier));
49 U_fourier(:,:,k) = U_fourier(:,:,k) + M_L(:,:,k).*term;
50 Mu_fourier(:,:,k) = Mu_fourier(:,:,k) - (Delta - alpha/epsilon^2).*M_L(:,:,k).*term;
51 U(:,:,k) = real(ifft2(U_fourier(:,:,k)));
52 Mu(:,:,k) = ifft2(Mu_fourier(:,:,k));
53 end
54 end

```

FIGURE 1. Example of **Matlab** implementation of our scheme in dimension 2 to approximate the solutions of model **MCH**.

where

$$H(u^n, \mu^n) = N(u^n) \operatorname{div}((M(u^n) \nabla(N(u^n) \mu^n)) - m \Delta \mu^n + \beta \mu^n).$$

Remark 3.3. Recall that this approach is based on the convex-concave splitting of the associated metric

$$\frac{1}{2} \int_Q M(u) |\nabla(N(u) \mu)|^2 dx = J_{u,c}(\mu) + J_{u,e}(\mu),$$

with

$$J_{u,c}(\mu) = \frac{1}{2} \int_Q m |\nabla \mu|^2 dx + \frac{1}{2} \int_Q \beta \mu^2 dx$$

and

$$J_{u,e}(\mu) = \int_Q G(u) \cdot \nabla \mu \mu dx + \frac{1}{2} \int_Q (|G(u)|^2 - \beta) \mu^2 dx + \frac{1}{2} \int_Q (1 - m) |\nabla \mu|^2 dx.$$

Here, $G(u) = -\frac{1}{2} \nabla(\log(M(u)))$, and as it is bounded is $H^1(Q)$, a sufficiently large choice for m and β should ensure the concavity of $J_{u,e}(\mu)$ and the stability of the scheme. In practice, we take $m = 1$ and $\beta = 1/\varepsilon^2$ for our numerical experiments and these values did not show any sign of instability regardless of the choice of the time step δ_t .

Finally, the couple (u^{n+1}, μ^{n+1}) is solution of the system

$$\begin{pmatrix} I_d & -\delta_t(m\Delta - \beta I_d) \\ \Delta - \alpha/\varepsilon^2 & I_d \end{pmatrix} \begin{pmatrix} u^{n+1} \\ \mu^{n+1} \end{pmatrix} = \begin{pmatrix} B_{u^n, \mu^n}^1 \\ B_{u^n, \mu^n}^2 \end{pmatrix},$$

with

$$\begin{pmatrix} B_{u^n, \mu^n}^1 \\ B_{u^n, \mu^n}^2 \end{pmatrix} = \begin{pmatrix} u^n + \delta_t H(u^n, \mu^n) \\ \frac{1}{\varepsilon^2} (W'(u^n) - \alpha u^n) \end{pmatrix},$$

and satisfies

$$\begin{cases} u^{n+1} &= L_{NMN} \left[B_{u^n, \mu^n}^1 + \delta_t (m \Delta B_{u^n, \mu^n}^2 - \beta B_{u^n, \mu^n}^2) \right] \\ \mu^{n+1} &= L_{NMN} \left[(-\Delta B_{u^n, \mu^n}^1 + \alpha/\varepsilon^2 B_{u^n, \mu^n}^1) + B_{u^n, \mu^n}^2 \right]. \end{cases}$$

Here the operator L_{NMN} is given by $L_{NMN} = (I_d + \delta_t(m\Delta - \beta I_d)(\Delta - \alpha/\varepsilon^2 I_d))^{-1}$, which can be still computed efficiently in Fourier space.

We now propose to extend this approach in the multi-phase case:

$$\begin{cases} \partial_t u_k &= \nu_k N(u_k) \operatorname{div} [M(u_k) \nabla [N(u_k) \sigma_k \mu_k + \lambda]] , \\ \mu_k &= \frac{W'(u_k)}{\varepsilon^2} - \Delta u_k, \\ 1 &= \sum_k u_k. \end{cases}$$

The scheme reads

$$\begin{cases} (u_k^{n+1} - u_k^n)/\delta_t &= \nu_k [m\Delta - \beta] (\sigma_k \mu_k^{n+1} + \lambda^{n+1}) + H_k(u_k^n, \mu_k^n, \lambda^n) \\ \mu_k^{n+1} &= \left(-\Delta u_k^{n+1} + \frac{\alpha}{\varepsilon^2} u_k^{n+1} \right) + \left(\frac{1}{\varepsilon^2} (W'(u_k^n) - \alpha u_k^n) \right), \end{cases}$$

where

$$H_k(u_k^n, \mu_k^n, \lambda^n) = \nu_k (N(u_k^n) \operatorname{div}((M(u_k^n) \nabla(N(u_k^n) (\sigma_k \mu_k^n + \lambda^n))) - [m\Delta - \beta] (\sigma_k \mu_k^n + \lambda^n)).$$

and λ^{n+1} defined to satisfy the partition constraint $\sum_k u_k^{n+1} = 1$.

Let us now introduce the couple $(u_k^{n+1/2}, \mu_k^{n+1/2})$ defined by

$$\begin{cases} u_k^{n+1/2} &= L_{NMN,k} \left[B_{u_k^n, \mu_k^n, \lambda^n}^1 + \delta_t \nu_k \sigma_k ([m\Delta - \beta] B_{u_k^n, \mu_k^n, \lambda^n}^2) \right] \\ \mu_k^{n+1/2} &= L_{NMN,k} \left[(-\Delta B_{u_k^n, \mu_k^n, \lambda^n}^1 + \alpha/\varepsilon^2 B_{u_k^n, \mu_k^n, \lambda^n}^1) + B_{u_k^n, \mu_k^n, \lambda^n}^2 \right]. \end{cases}$$

where

$$L_{NMN,k} = \left(I_d + \delta_t \nu_k \sigma_k (m\Delta - \beta I_d) (\Delta - \alpha/\varepsilon^2 I_d) \right)^{-1}$$

and

$$B_{u^n, \mu^n, \lambda^n}^1 = u^n + \delta_t H(u^n, \mu^n, \lambda^n) \text{ and } B_{u^n, \mu^n, \lambda^n}^2 = \frac{1}{\varepsilon^2} (W'(u^n) - \alpha u^n).$$

Finally, it is not difficult to see that

$$\begin{cases} u_k^{n+1} &= u_k^{n+1/2} + \delta_t \nu_k L_{NMN,k} [m\Delta - \beta] \lambda^{n+1} \\ \mu_k^{n+1} &= \mu_k^{n+1/2} + \delta_t \nu_k L_{NMN,k} \left[(-\Delta + \frac{\alpha}{\varepsilon^2}) (m\Delta - \beta) \lambda^{n+1} \right] \end{cases}$$

which shows that λ^{n+1} satisfies

$$\lambda^{n+1} = \frac{1}{\delta_t} \left[\sum_k \nu_k L_{NMN,k} (m\Delta - \beta) \right]^{-1} \left(1 - \sum_k u_k^{n+1/2} \right).$$

where the operator $[\sum_k \nu_k L_{NMN,k} (m\Delta - \beta)]^{-1}$ is still homogeneous and can be computed easily in Fourier space.

Similarly to model **MCH**, the implementation of previous scheme is simple and efficient. We present in Figure (2) an example of **Matlab** script with less than 60 lines which implements the scheme approximating the solutions of the **NMNCH** model. In particular :

- We consider here a computation box $Q = [-1/2, 1/2]^2$ discretized with $N = 2^8$ nodes in each direction. The initial condition of u is a uniform noise and the numerical parameters are given by $\varepsilon = 1/N$, $\delta_t = \varepsilon^4$, $\alpha = 2$, $\beta = 2/\varepsilon^2$ and $m = 1$.
- The implementation is identical to the previous model. Only the treatment of the term in divergence $H_k(u_k^n, \mu_k^n, \lambda^n)$ is changed. This is done in lines 33 to 36 and is based on the following equality:

$$\begin{aligned} N(u) \operatorname{div}(M(u) \nabla(N(u)\mu)) &= \sqrt{M(u)\Delta} (N(u)\mu) + N(u) \nabla(M(u)) \cdot \nabla(N(u)\mu) \\ &= \sqrt{M(u)\Delta} (N(u)\mu) + 2\nabla \left[\sqrt{M(u)} \right] \cdot \nabla(N(u)\mu), \end{aligned}$$

as $N(u) = 1/\sqrt{M(u)}$. See [17] for more details.

- Figure (3) shows the function $u_2^n + 2u_3^n$ computed at different times t^n by using this script.

We believe that our previous implementations show the simplicity, efficiency and stability of our numerical scheme.

3.4. Numerical validation of our approach.

3.4.1. Asymptotic expansion and flow: numerical comparison of the two different models.

The first numerical example concerns the evolution of an initial connected set. For each Cahn–Hilliard model, we plot on figure (4) the phase field function $u_2^n + 2u_3^n$ computed at different times t . Each experiment is performed using the same numerical parameters: $N = 2^8$, $\varepsilon = \delta_x$, $\delta_t = \varepsilon^4$, $\alpha = 2$, $m = 1$, and $\beta = 2/\varepsilon^2$.

The first and second lines on (4) correspond respectively to the solution u given by the **MCH** model and the **NMNCH** model. Notice that the numerical experiments obtained using the **MCH** model and the **NMNCH** model are very similar and should give a good approximation of the surface diffusion flow. In addition, for each model, the stationary flow limit appears to correspond to a ball of the same mass as that of the initial set.

To illustrate the asymptotic expansion performed in Section 2, we plot on (5) (first two pictures) the slice $x_1 \mapsto u_1(x_1, 0)$ at the final time $T = 10^{-4}$. The profile associated to the **MCH** model is plotted in red and clearly indicates that the solution u does not remain in the interval

```

1 clear all;
2 %%%%%%%%%%%%%%%%%%%%%%%%%%%%%%%%%%%%%%%%%%%%%%%%%%%%%%%%%%%%%%%%%%%%%%%%% parameters %%%%%%%%%%%%%%%%%%%%%%%%%%%%%%%%%%%%%%%%%%%%%%%%%%%%%%%%%%%%%%%%%%%%%%%%%
3 N = 2^8; epsilon =1/N; dt = epsilon^4; T = 10^(-4);
4 alpha = 2; gamma=1; beta = 2/epsilon^2;
5 W_prim = @(U) (U.*(U-1).*(2*U-1));
6 MobM = @(U) 1/2*(((U).*(1-U)).^2+epsilon^2 );
7 MobN = @(U) 1./sqrt(MobM(U) );
8 %%%%%%%%%%%%%%%%%%%%%%%%%%%%%%%%%%%%%%%%%%%%%%%%%%%%%%%%%%%%%%%%%%%%%%%%% initial condition %%%%%%%%%%%%%%%%%%%%%%%%%%%%%%%%%%%%%%%%%%%%%%%%%%%%%%%%%%%%%%%%%%%%%%%%%
9 U(:, :,1) = 2*rand(N,N)/3; U(:, :,2) = rand(N,N).*(1 -U(:, :,1) );
10 U(:, :,3) = 1-(U(:, :,1) + U(:, :,2) );
11 Mu = 0*U; lambda = 0; lambda_fourier = 0; Mu_fourier = zeros(N,N,3);
12 for k=1:3, U_fourier(:, :,k) = fft2(U(:, :,k)); end
13 %%%%%%%%%%%%%%%%%%%%%%%%%%%%%%%%%%%%%%%%%%%%%%%%%%%%%%%%%%%%%%%%%%%%%%%%% surface tension coefficients - mobilities %%%%%%%%%%%%%%%%%%%%%%%%%%%%%%%%%%%%%%%%%%%%%%%%%%%%%%%%%%%%%%%%%%%%%%%%%
14 sigma12 =1; sigma13 =1; sigma23 =1;
15 sigma(1) = (sigma12 + sigma13 - sigma23)/2;
16 sigma(2) = (sigma12 + sigma23 - sigma13)/2;
17 sigma(3) = (sigma23 + sigma13 - sigma12)/2;
18 mob(1) = 1; mob(2)= 1; mob(3) = 1;
19 %%%%%%%%%%%%%%%%%%%%%%%%%%%%%%%%%%%%%%%%%%%%%%%%%%%%%%%%%%%%%%%%%%%%%%%%% Kernel %%%%%%%%%%%%%%%%%%%%%%%%%%%%%%%%%%%%%%%%%%%%%%%%%%%%%%%%%%%%%%%%%%%%%%%%%
20 k = [0:N/2,-N/2+1:-1]; [K1,K2] = meshgrid(k,k);
21 Delta = -4*pi^2*((K1.^2 + (K2).^2)); M_L = zeros(N,N,3);
22 for k=1:3,
23 M_L(:, :,k) = 1./(1 + dt*sigma(k)*mob(k)*(gamma*Delta - beta) .*(Delta - alpha/epsilon
    ^2));
24 end
25 %%%%%%%%%%%%%%%%%%%%%%%%%%%%%%%%%%%%%%%%%%%%%%%%%%%%%%%%%%%%%%%%%%%%%%%%%loop %%%%%%%%%%%%%%%%%%%%%%%%%%%%%%%%%%%%%%%%%%%%%%%%%%%%%%%%%%%%%%%%%%%%%%%%%
26 for i=1:T/dt,
27 %%%%%%%%%%%%%%%%%%%%%%%%%%%%%%%%%%%%%%%%%%%%%%%%%%%%%%%%%%%%%%%%%%%%%%%%% computation of u^{n+1/2}_k, \mu^{n+1/2}_k
28 for k=1:3,
29 mobMUk = MobM(U(:, :,k)); mobNUk = MobN(U(:, :,k));
30 sqrtMk = sqrt(mobMUk); sqrtMk_fourier = fft2(sqrtMk);
31 nabla1_sqrtMk= real(ifft2(2*pi*1i*K1.*sqrtMk_fourier )); nabla2_sqrtMk= real(ifft2(2*
    pi*1i*K2.*sqrtMk_fourier ));
32 muN_fourier = fft2((sigma(k)*Mu(:, :,k) + lambda).*mobNUk);
33 nabla1_muN = real(ifft2(2*pi*1i*K1.*muN_fourier ));
34 nabla2_muN = real(ifft2(2*pi*1i*K2.*muN_fourier ));
35 laplacien_muN = real(ifft2(Delta.*muN_fourier ));
36 NdivMgradNMu = sqrtMk.*laplacien_muN + 2*(nabla1_sqrtMk.*nabla1_muN +nabla2_sqrtMk.*
    nabla2_muN);
37 B1 = U_fourier(:, :,k) + dt*(mob(k)*fft2(NdivMgradNMu) - mob(k)*(gamma*Delta-beta).*((
    sigma(k)*Mu_fourier(:, :,k)+lambda_fourier)));
38 B2 = fft2(W_prim(U(:, :,k))/epsilon^2 - alpha/epsilon^2*U(:, :,k));
39 U_fourier(:, :,k) = M_L(:, :,k).*(B1 + dt*mob(k)*sigma(k)*(gamma*Delta-beta).*B2);
40 U(:, :,k) = real(ifft2(U_fourier(:, :,k)));
41 Mu_fourier(:, :,k) = M_L(:, :,k).*((alpha/epsilon^2 - Delta).*B1 + B2);
42 Mu(:, :,k) = real(ifft2(Mu_fourier(:, :,k)));
43 end
44 %%%%%%%%%%%%%%%%%%%%%%%%%%%%%%%%%%%%%%%%%%%%%%%%%%%%%%%%%%%%%%%%%%%%%%%%% computation of lambda and correction %%%%%%%%%%%%%%%%%%%%%%%%%%%%%%%%%%%%%%%%%%%%%%%%%%%%%%%%%%%%%%%%%%%%%%%%%
45 Err_sum = fft2(1 - sum(U,3));
46 weight = (M_L(:, :,1)*mob(1) +M_L(:, :,2)*mob(2) + M_L(:, :,3)*mob(3)).*(gamma*Delta-1*
    beta);
47 lambda_fourier = (1./(weight)).*Err_sum/dt;
48 lambda = real(ifft2(lambda_fourier));
49 for k=1:3,
50 term = (mob(k)*M_L(:, :,k)./((M_L(:, :,1)*mob(1) +M_L(:, :,2)*mob(2) + M_L(:, :,3)*mob(3))
    )).*Err_sum;
51 U_fourier(:, :,k) = U_fourier(:, :,k) + term;
52 Mu_fourier(:, :,k) = Mu_fourier(:, :,k) - (Delta - alpha/epsilon^2).*term;
53 U(:, :,k) = real(ifft2(U_fourier(:, :,k))); 23
54 Mu(:, :,k) = real(ifft2(Mu_fourier(:, :,k)));
55 end
56 end

```

FIGURE 2. Example of **Matlab** implementation of our scheme in dimension 2

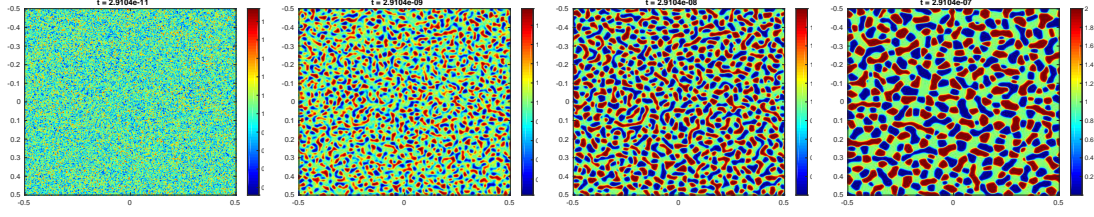


FIGURE 3. First numerical experiment using the **NMN-CH** model; the solutions u are computed with the **Matlab** script of Figure 2. We plot the function $x \mapsto u_2(x) + 2u_3(x)$ on each picture which means that the phase one, two and three appear respectively in blue, green and red.

$[0, 1]$ with an overshoot of order $O(\varepsilon)$. In contrast, the profile obtained using the **NMNCH** model (in green) seems to be very close to q and remains in $[0, 1]$ up to an error of order $O(\varepsilon^2)$. Finally, we plot the evolution of the Cahn–Hilliard energy along the flow for each model on the last picture of (5). We can clearly observe a decrease of the energy in each case.

In conclusion, this first numerical experiment confirms the asymptotic expansion obtained in the previous section, and highlights the interest of our **NMNCH** model to approximate surface diffusion flows.

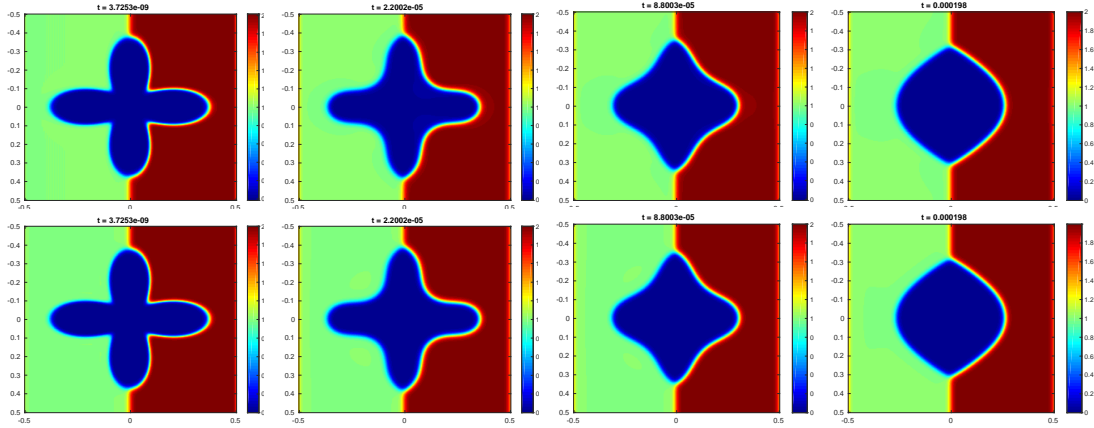


FIGURE 4. First numerical comparison of the two different **CH** models: Evolution of u along the iterations. First line using **MCH**, Second line, using **NMNCH**.

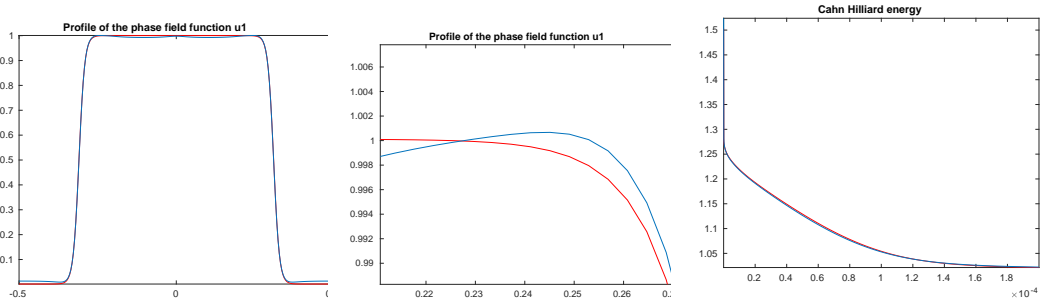


FIGURE 5. Comparison of the two different models: profil and energy; **MCH** in blue, **NMNCH** in red; First figure: slice of u : $x_1 \mapsto u_1(x_1, 0)$; Second figure: zoom on the slice of u_1 ; last figure: evolution of the Cahn–Hilliard energy along the flow.

3.4.2. Influence of the mobility using model **NMNCH**.

The second numerical experiment is intended to show the influence of surface mobilities (ν_{ij}) only on the velocity of each interface. To illustrate this, we show in (6) the evolution of \mathbf{u} in two different cases: a first case where $\nu_i = 1$ (see first row in (6)); a second case where $\nu_2 = \nu_3 = 1$ and $\nu_1 = 0$ (see second row in (6)). In both cases, coefficients (σ_i) associated with surface tensions (σ_{ij}) are set to $\sigma_i = 1$. As previously, we use the same numerical parameters in each case, we take $N = 2^8$, $\varepsilon = 2/N$, $\delta_t = \varepsilon^4$, $\alpha = 2$, $m = 1$, and $\beta = 2/\varepsilon^2$.

As expected, we observe in the first row of figure (6) that all phases are active along iterations since the mobility coefficients ν_i are all equal to 1. On the contrary, in the second row, the first phase (u_1 in blue) is fixed along iterations, which is consistent with the fact that the coefficient mobility associated with the first phase u_1 is $\nu_1 = 0$. Indeed, it is important to notice that mobilities play a role only in the gradient flow and therefore imposing zero mobility $\nu_k = 0$ forces the k -th phase u_k to be fixed. In particular, this allows us to deal easily and efficiently with the Cahn-Hilliard problem in irregular domain and the second row of (6) is a perfect illustration of it. We insist that our model does not impose any boundary conditions on the complex domain, nor the insertion of surface energy. See [64, 50, 69, 48, 75] for some details of this application. Another important remark is that the width of the diffuse interface depends only on ε and not depend neither on the surface tensions nor on mobilities.

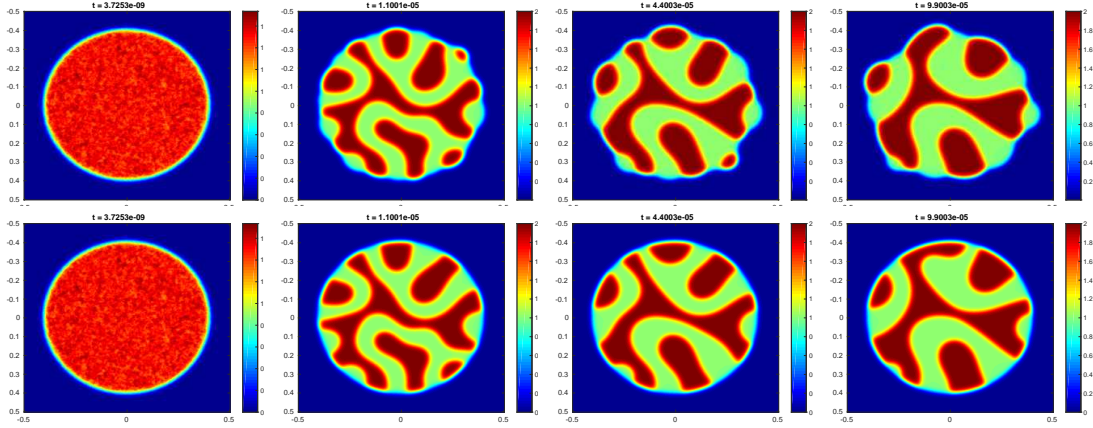


FIGURE 6. Influence of the mobility using **NMNCH**: Evolution of \mathbf{u} along the iterations; First line using $\nu_1 = \nu_2 = \nu_3 = 1$, Second line, using $\nu_1 = 0$ and $\nu_2 = \nu_3 = 1$

3.4.3. Influence of the surface tension coefficients using the model **NMNCH**.

Model **NMNCH** can also handle the case of the evolution of a liquid phase on a fixed solid surface by simply imposing null mobility of the solid interface. Here we propose an application in space dimension 2. Figure (7) illustrates numerical results obtained with different sets of surface tension coefficients $\sigma = (\sigma_{12}, \sigma_{13}, \sigma_{23})$, with mobilities $\nu_1 = 0$, $\nu_2 = \nu_3 = 1$ and the same initial condition: $\sigma = (1, 1, 1)$, $\sigma = (1.9, 1, 1)$ and $\sigma = (1, 1.9, 1)$ for the first, the second and the third row of (7) respectively. The solid u_1 , liquid u_2 and vapor u_3 phases are represented in blue, red and green respectively. Similarly to the previous computations, the numerical parameters are given by $N = 2^8$, $\varepsilon = 2/N$, $\delta_t = \varepsilon^4$, $\alpha = 2$, $m = 1$, and $\beta = 2/\varepsilon^2$. As in the previous numerical experiment, we notice the ability of our model to treat the case of null mobilities (here to fix the exterior solid phase u_1 in blue). In Figure (7), we can also see the strong influence of the contact angle on the evolution of the liquid phase. We emphasize that our model does not prescribe the contact angle. Rather, its value is a direct consequence of the multiphase interface energy considered in each simulation.

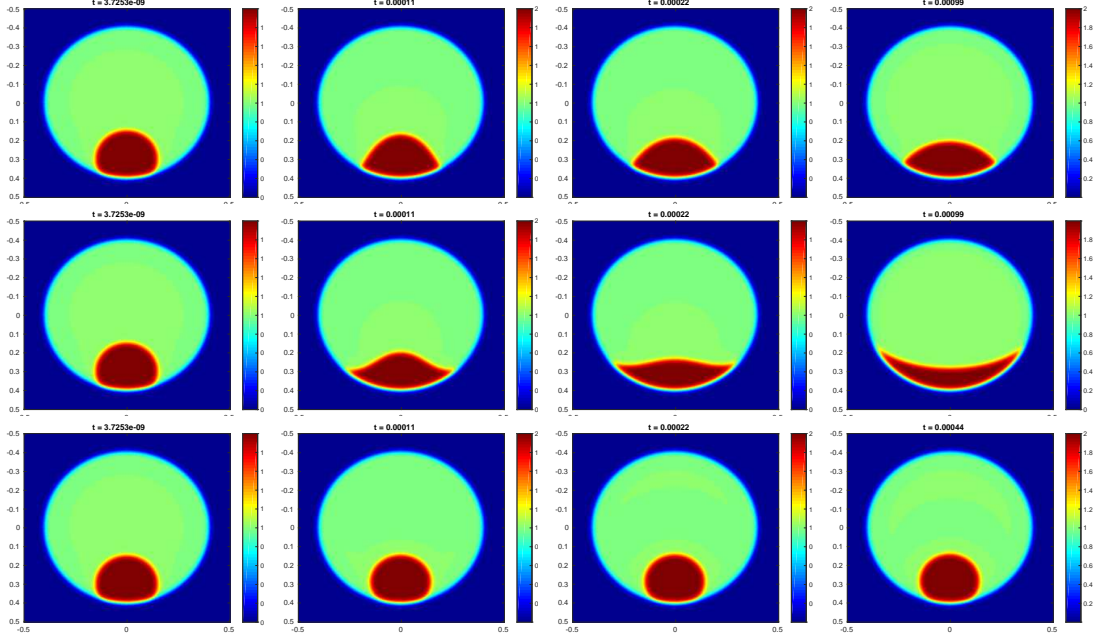


FIGURE 7. Influence of the surface tension coefficients using NMNCH: Evolution of \mathbf{u} along the iterations; First line using $\sigma_{12} = \sigma_{13} = \sigma_{23} = 1$, Second line, using $\sigma_{12} = 1.9$ and $\sigma_{13} = \sigma_{23} = 1$, Third line, using $\sigma_{13} = 1.9$ and $\sigma_{12} = \sigma_{23} = 1$

4. APPLICATION FOR WETTING OR DEWETTING PHENOMENEA

Let's recall that the behavior of liquids on solid surfaces has been of interest to the academic and engineering communities for many decades. Young [76] determined the optimal shape of a drop in equilibrium on a solid surface. More precisely, the shape of the drop can be seen as the solution to the following energy minimization

$$P(\Omega_L) = \int_{\Gamma_{L,S}} \sigma_{L,S} \mathcal{H}^{d-1} + \int_{\Gamma_{L,V}} \sigma_{L,V} d\mathcal{H}^{d-1} + \int_{\Gamma_{L,V}} \sigma_{S,V} \mathcal{H}^{d-1},$$

under a constraint on the volume of the set Ω_L which represents the droplet. Here, $\sigma_{L,S}$, $\sigma_{L,V}$ and $\sigma_{S,V}$ are the surface tensions between liquid (L), solid (S), and vapor (S) phases. In particular, the minimizers of this energy satisfy Young's law for the contact angle θ of the droplet on the solid.

$$\cos(\theta) = \frac{\sigma_{S,V} - \sigma_{S,L}}{\sigma_{L,V}}.$$

As illustrated in the figure (7), the approximation of such an evolution can be obtained by using the previous phase field model with the following set of mobilities: $\nu_{LV} = 1$ and $\nu_{SV} = \nu_{SL} = 0$.

Other approaches have been developed, such as [19] where Cahn proposed a phase-field approach to model the situation in [19] using a additional surface energy on the boundary of the solid phase. However, this method is only applicable for contact angles $\theta < \frac{\pi}{2}$. An approach using the smoothed boundary conditions in order to force the correct contact angle condition is available in [70] within the Allen-Cahn equation context. Other methods relying on the Allen-Cahn equation using this idea are proposed in [8, 29]. Other methods using a wall components boundary conditions with a third order polynomial to impose the contact angle have been proposed in [67, 68, 5]. A convexity splitting scheme using this idea with a sinusoidal boundary condition can be found in [72]. In [30, 54, 22, 63, 12] the angle is imposed by using a wall components boundary conditions as mentionned in the previous paragraph. The dynamic case can be treated via a coupled Cahn-Hilliard/Navier-Stokes system. In most cases, see for example [38, 51, 70, 1, 10], the contact angle is fixed to the static contact angle $\frac{\pi}{2}$.

In the convolution-thresholding framework, some recent approaches have been proposed to simulate the wetting phenomenon. Expanding the original scheme of Merriman, Bence and Osher [53], Esedoglu and Otto have proposed a multiphase convolution-thresholding method in [34] for arbitrary surface tensions satisfying the triangle inequality. Wang et al. then applied this generalization to the Wetting case in [71]. A different approach proposed in [74] does not impose the contact angle in the formulation but requires the use of sophisticated techniques while solving the heat equation.

In [15, 14], two of the authors proposed an Allen-Cahn equation where the solid phase was frozen in order to approximate droplet wetting. It was based on the use of zero surface mobilities for the solid-vapor and solid-liquid interfaces. In this paper, we extend this idea to the Cahn-Hilliard equation and, coupled with a reformulation of the problem, we introduce a new simple and efficient method for simulating the wetting phenomenon. It is important to emphasize that this method does not impose the contact angle, which is determined implicitly by the surface tension coefficients $(\sigma_{S,V}, \sigma_{S,L}, \sigma_{L,V})$.

4.1. Rewriting of our phase field approach using the liquid phase only.

The motivation of this section is to present an equivalent phase field model using only one phase, the liquid phase, as Ω_S is fixed and Ω_V can be obtained from Ω_L and Ω_S . Indeed, numerical experiment in dimension 3 of a complete model (u_L, u_V, u_S) can be quite challenging numerically and it may be preferable to reduce the system to the only unknown, the liquid phase.

Recall that in such case, the Cahn Hilliard energy reads as

$$P_\varepsilon(\mathbf{u}) = \sum_{k \in \{S, L, V\}} \frac{\sigma_k}{2} \int_Q \frac{\varepsilon}{2} |\nabla u_k|^2 + \frac{1}{\varepsilon} W(u_k),$$

where

$$\sigma_L = \frac{\sigma_{LS} + \sigma_{LV} - \sigma_{SV}}{2}, \sigma_S = \frac{\sigma_{LS} + \sigma_{SV} - \sigma_{LV}}{2} \text{ and } \sigma_V = \frac{\sigma_{LV} + \sigma_{SV} - \sigma_{LS}}{2}.$$

Here, u_S represents the phase field function associated to the solid set Ω_S and the previous asymptotic developments show that u_S should be of the form $u_S = q\left(\frac{\text{dist}(x, \Omega_S)}{\varepsilon}\right)$. On the other hand, the vapor phase field function u_V can be obtained using the partition constraint with $u_V = 1 - (u_S + u_L)$. The Cahn-Hilliard energy can then be rewritten using only the variable u_L as follows:

$$\begin{aligned} \tilde{P}_\varepsilon(u_L) &= \frac{\sigma_L}{2} \int_Q \frac{\varepsilon}{2} |\nabla u_L|^2 + \frac{1}{\varepsilon} W(u_L) \\ &+ \frac{\sigma_V}{2} \int_Q \frac{\varepsilon}{2} |\nabla(1 - (u_S + u_L))|^2 + \frac{1}{\varepsilon} W(1 - (u_L + u_S)) \\ &+ \frac{\sigma_S}{2} \int_Q \frac{\varepsilon}{2} |\nabla u_S|^2 + \frac{1}{\varepsilon} W(u_S). \end{aligned}$$

Notice that its L^2 -gradient satisfies

$$\nabla_{L^2} \tilde{P}_\varepsilon(u_L) = \frac{\sigma_{SL}}{2} [-\varepsilon \Delta u_L + \frac{1}{\varepsilon} W'(u_L)] + \frac{\sigma_V}{2} \varepsilon R_{u_S}(u_L)$$

where the first term

$$\frac{\sigma_{SL}}{2} [-\varepsilon \Delta u_L + \frac{1}{\varepsilon} W'(u_L)],$$

is a classical Allen Cahn term and the second term one

$$R_{u_S}(u_L) = - \left[\Delta u_S + \frac{1}{\varepsilon^2} (W'(u_L) + W'(1 - (u_L + u_S))) \right],$$

appears as a smooth penalization term which is active only on the boundary of Ω_S .

Finally, adding mobilities, this leads us to consider the following two Cahn Hilliard models:

- **MCH model**

$$\begin{cases} \partial_t u_L &= \operatorname{div} (M(u_k) \nabla (\sigma_{LV}/2 \mu_L + \sigma_V R_{u_S}(u_L))) \\ \mu_L &= \frac{W'(u_L)}{\varepsilon^2} - \Delta u_L \end{cases}$$

- **NMNCH model**

$$\begin{cases} \partial_t u_L &= N(u_L) \operatorname{div} (M(u_L) \nabla (N(u_L) (\sigma_{LV}/2 \mu_L + \sigma_V R_{u_S}(u_L)))) \\ \mu_L &= \frac{W'(u_L)}{\varepsilon^2} - \Delta u_L \end{cases}$$

Note that in practice, we will only use here the **NMNCH** model for our simulations because the wetting problem of a thin structure requires to have a model as precise as possible.

About numerical scheme, the idea is to apply the previous scheme with an explicit treatment of the penalization term $R_{u_S}(u_L)$.

Notice also that the penalization term $R_{u_S}(u_L)$ is active on all the boundary of Ω_S . In particular, when $u_L = 0$ this term is still active and can be important as it corresponds to the Allen Cahn term associated to u_S :

$$R_{u_S}(u_L) = - \left(\Delta u_S + \frac{1}{\varepsilon^2} W'(1 - u_S) \right) = -\Delta u_S - \frac{1}{\varepsilon^2} W'(u_S).$$

In practice, we propose to locate it only at the liquid phase boundary u_L , which can be done by considering the following variant

$$\tilde{R}_{u_S}(u_L) = R_{u_S}(u_L) \frac{\sqrt{2W(u_L)}}{\sqrt{2W(u_L)} + \varepsilon}.$$

The interest is then to stabilize the numerical scheme without disturbing the evolution of the liquid phase.

4.2. Influence of the surface tension coefficients.

We now propose a numerical experiment in dimension 3 where the initial set is a thin tube. The numerical parameters are given by $N = 2^8$, $\varepsilon = 1/N$, $\delta_t = \varepsilon^4$, $\alpha = 2$, $m = 1$, and $\beta = 2/\varepsilon^2$. We plot on each picture of figure (8) the phase field function $u_2^n + 2u_3^n$ computed at different times t . As in 2D case, surface tension coefficients have a considerable influence on the evolution of the liquid phase. They affect both the wetting rate and the final shape of the liquid phase.

4.3. Influence of the roughness of the solid support.

Our approach is able to easily consider solid supports with roughness. In (9), we test the case of a classical flat support, one with randomly generated roughness and an oscillatory one. We then observe a direct influence of the substrate roughness on the wetting dynamics, each simulation being initialized in a similar way and using the same set of coefficients.

ACKNOWLEDGMENT

The authors acknowledge support from the French National Research Agency (ANR) under grants ANR-18-CE05-0017 (project BEEP) and ANR-19-CE01-0009-01 (project MIMESIS-3D). Part of this work was also supported by the LABEX MILYON (ANR-10-LABX-0070) of Université de Lyon, within the program "Investissements d'Avenir" (ANR-11-IDEX- 0007) operated by the French National Research Agency (ANR).

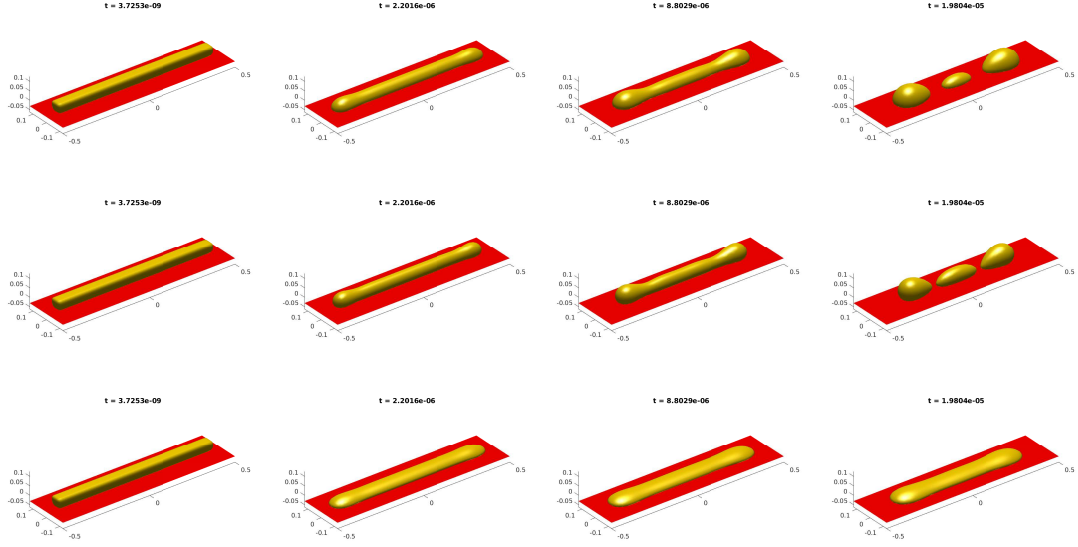


FIGURE 8. Influence of the surface tension coefficients using the **NMNCH** model: Evolution of \mathbf{u} along the iterations; First line using $\sigma_{LV} = \sigma_{VS} = \sigma_{SL} = 1$, Second line, using $\sigma_{LS} = 1.7$ and $\sigma_{LV} = \sigma_{VS} = 1$, Third line, using $\sigma_{VS} = 1.7$ and $\sigma_{LV} = \sigma_{LS} = 1$.

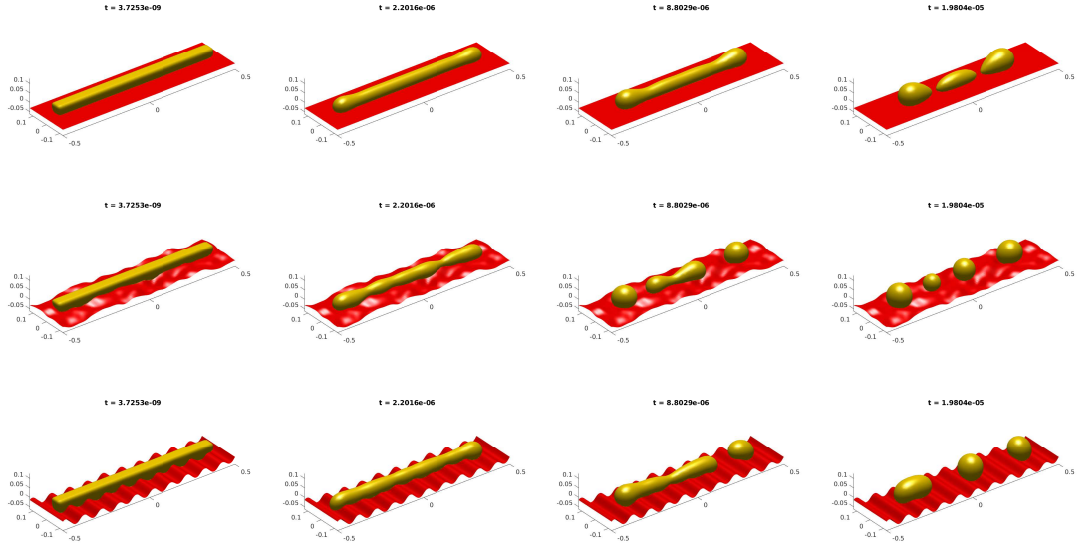


FIGURE 9. Influence of the roughness of the solid support using the **NMNCH** model: Evolution of \mathbf{u} along the iterations using $\sigma_{LS} = 1.7$ and $\sigma_{LV} = \sigma_{VS} = 1$.

REFERENCES

- [1] Helmut Abels. On a diffuse interface model for two-phase flows of viscous, incompressible fluids with matched densities. *Archive for rational mechanics and analysis*, 194(2):463–506, 2009. [26](#)
- [2] Marco Albani, Roberto Bergamaschini, and Francesco Montalenti. Dynamics of pit filling in heteroepitaxy via phase-field simulations. *Physical Review B*, 94(7):075303, 2016. [3](#)
- [3] Matthieu Alfaro and Pierre Alifrangis. Convergence of a mass conserving allen-cahn equation whose lagrange multiplier is nonlocal and local. *arXiv preprint arXiv:1303.3553*, 2013. [5](#)
- [4] Nicholas D Alikakos, Peter W Bates, and Xinfu Chen. Convergence of the cahn-hilliard equation to the hele-shaw model. *Archive for rational mechanics and analysis*, 128(2):165–205, 1994. [3](#)

- [5] Benjamin Aymard, Urbain Vaes, Marc Pradas, and Serafim Kalliadasis. A linear, second-order, energy stable, fully adaptive finite element method for phase-field modelling of wetting phenomena. *Journal of Computational Physics: X*, 2:100010, 2019. [26](#)
- [6] Rainer Backofen, Steven M Wise, Marco Salvalaglio, and Axel Voigt. Convexity splitting in a phase field model for surface diffusion. *arXiv preprint arXiv:1710.09675*, 2017. [16](#)
- [7] John W. Barrett, Harald Garcke, and Robert Nürnberg. A parametric finite element method for fourth order geometric evolution equations. *Journal of Computational Physics*, 222(1):441–467, March 2007. [16](#)
- [8] Marouen Ben Said, Michael Selzer, Britta Nestler, Daniel Braun, Christian Greiner, and Harald Garcke. A phase-field approach for wetting phenomena of multiphase droplets on solid surfaces. *Langmuir*, 30(14):4033–4039, 2014. [26](#)
- [9] Saswata Bhattacharyya and T. A. Abinandanan. A study of phase separation in ternary alloys. *Bull Mater Sci*, 26(1):193–197, January 2003. [16](#)
- [10] Franck Boyer, Céline Lapuerta, Sebastian Minjeaud, Bruno Piar, and Michel Quintard. Cahn–hilliard/navier–stokes model for the simulation of three-phase flows. *Transport in Porous Media*, 82(3):463–483, 2010. [26](#)
- [11] Franck Boyer and Céline Lapuerta. Study of a three component Cahn-Hilliard flow model. *ESAIM: M2AN*, 40(4):653–687, July 2006. [16](#)
- [12] Franck Boyer and Flore Nabet. A ddfv method for a cahn- hilliard/stokes phase field model with dynamic boundary conditions. *ESAIM: Mathematical Modelling and Numerical Analysis*, 51(5):1691–1731, 2017. [26](#)
- [13] M. Brassel and E. Bretin. A modified phase field approximation for mean curvature flow with conservation of the volume. *Mathematical Methods in the Applied Sciences*, 34(10):1157–1180, 2011. [16](#)
- [14] Elie Bretin, Alexandre Danescu, José Penuelas, and Simon Masnou. Multiphase mean curvature flows with high mobility contrasts: a phase-field approach, with applications to nanowires. *Journal of Computational Physics*, 365:324–349, 2018. [2](#), [4](#), [16](#), [27](#)
- [15] Elie Bretin and Simon Masnou. A new phase field model for inhomogeneous minimal partitions, and applications to droplets dynamics. *Interfaces and Free Boundaries*, 19(2):141–182, 2017. [16](#), [27](#)
- [16] Elie Bretin, Simon Masnou, and Édouard Oudet. Phase-field approximations of the Willmore functional and flow. *Numer. Math.*, 131(1):115–171, 2015. [5](#)
- [17] Elie Bretin, Simon Masnou, Arnaud Sengers, and Garry Terii. Approximation of surface diffusion flow: a second order variational cahn–hilliard model with degenerate mobilities. *arXiv preprint arXiv:2007.03793*, 2020. [1](#), [2](#), [3](#), [4](#), [5](#), [16](#), [17](#), [18](#), [19](#), [22](#)
- [18] Bretin, Élie, Denis, Roland, Lachaud, Jacques-Olivier, and Oudet, Édouard. Phase-field modelling and computing for a large number of phases. *ESAIM: M2AN*, 53(3):805–832, 2019. [16](#)
- [19] John W Cahn. Critical point wetting. *The Journal of Chemical Physics*, 66(8):3667–3672, 1977. [26](#)
- [20] John W Cahn, Charles M Elliott, and Amy Novick-Cohen. The cahn–hilliard equation with a concentration dependent mobility: motion by minus the laplacian of the mean curvature. *European journal of applied mathematics*, 7(3):287–301, 1996. [3](#)
- [21] David G Caraballo. The triangle inequalities and lower semi-continuity of surface energy of partitions. *Proceedings. Section A, Mathematics-The Royal Society of Edinburgh*, 139(3):449, 2009. [1](#)
- [22] Andreas Carlson, Minh Do-Quang, and Gustav Amberg. Dissipation in rapid dynamic wetting. *Journal of Fluid Mechanics*, 682:213–240, 2011. [26](#)
- [23] L.Q. Chen and Jie Shen. Applications of semi-implicit fourier-spectral method to phase field equations. *Computer Physics Communications*, 108:147–158, 1998. [16](#)
- [24] Xinfu Chen, Danielle Hilhorst, and Elisabeth Logak. Mass conserving allen–cahn equation and volume preserving mean curvature flow. *Interfaces and Free Boundaries*, 12(4):527–549, 2011. [5](#)
- [25] Mowei Cheng and James A. Warren. An efficient algorithm for solving the phase field crystal model. *J. Comput. Phys.*, 227(12):6241–6248, 2008. [16](#)
- [26] M.I.M. Copetti. Numerical experiments of phase separation in ternary mixtures. *Mathematics and Computers in Simulation*, 52(1):41–51, March 2000. [16](#)
- [27] Shibin Dai and Qiang Du. Motion of interfaces governed by the cahn–hilliard equation with highly disparate diffusion mobility. *SIAM Journal on Applied Mathematics*, 72(6):1818–1841, 2012. [3](#)
- [28] Shibin Dai and Qiang Du. Coarsening mechanism for systems governed by the cahn–hilliard equation with degenerate diffusion mobility. *Multiscale Modeling & Simulation*, 12(4):1870–1889, 2014. [3](#)
- [29] Felix Diewald, Charlotte Kuhn, Michaela Heier, Kai Langenbach, Martin Horsch, Hans Hasse, and Ralf Müller. Investigating the stability of the phase field solution of equilibrium droplet configurations by eigenvalues and eigenvectors. *Computational Materials Science*, 141:185–192, 2018. [26](#)
- [30] S Dong. On imposing dynamic contact-angle boundary conditions for wall-bounded liquid–gas flows. *Computer Methods in Applied Mechanics and Engineering*, 247:179–200, 2012. [26](#)
- [31] Qiang Du and Xiaobing Feng. Chapter 5 - the phase field method for geometric moving interfaces and their numerical approximations. In Andrea Bonito and Ricardo H. Nochetto, editors, *Geometric Partial Differential Equations - Part I*, volume 21 of *Handbook of Numerical Analysis*, page 425–508. Elsevier, 2020. [16](#)

- [32] Marion Dziwnik, Andreas Münch, and Barbara Wagner. An anisotropic phase-field model for solid-state dewetting and its sharp-interface limit. *Nonlinearity*, 30(4):1465, 2017. [3](#)
- [33] Matt Elsey and Benedikt Wirth. A simple and efficient scheme for phase field crystal simulation. *ESAIM Math. Model. Numer. Anal.*, 47(5):1413–1432, 2013. [16](#)
- [34] Selim Esedoglu and Felix Otto. Threshold dynamics for networks with arbitrary surface tensions. *Communications on pure and applied mathematics*, 68(5):808–864, 2015. [27](#)
- [35] David J. Eyre. Unconditionally gradient stable time marching the Cahn-Hilliard equation. In *Computational and mathematical models of microstructural evolution (San Francisco, CA, 1998)*, volume 529 of *Mater. Res. Soc. Sympos. Proc.*, pages 39–46. MRS, Warrendale, PA, 1998. [4](#), [16](#)
- [36] Hector Gomez and Thomas J. R. Hughes. Provably unconditionally stable, second-order time-accurate, mixed variational methods for phase-field models. *J. Comput. Phys.*, 230(13):5310–5327, 2011. [16](#)
- [37] Clemens Gugenberger, Robert Spatschek, and Klaus Kassner. Comparison of phase-field models for surface diffusion. *Physical Review E*, 78(1):016703, 2008. [3](#)
- [38] David Jacqmin. Calculation of two-phase navier–stokes flows using phase-field modeling. *Journal of Computational Physics*, 155(1):96–127, 1999. [26](#)
- [39] Kyungkeun Kang, Junseok Kim, and John Lowengrub. Conservative multigrid methods for ternary Cahn-Hilliard systems. *Communications in Mathematical Sciences*, 2(1):53–77, 2004. [16](#)
- [40] Junseok Kim. Phase field computations for ternary fluid flows. *Computer Methods in Applied Mechanics and Engineering*, 196(45-48):4779–4788, September 2007. [16](#)
- [41] Junseok Kim. A generalized continuous surface tension force formulation for phase-field models for multi-component immiscible fluid flows. *Computer Methods in Applied Mechanics and Engineering*, 198(37-40):3105–3112, August 2009. [16](#)
- [42] Junseok Kim and Kyungkeun Kang. A numerical method for the ternary Cahn–Hilliard system with a degenerate mobility. *Applied Numerical Mathematics*, 59(5):1029–1042, May 2009. [16](#)
- [43] Tomonori Kitashima, Jincheng Wang, and Hiroshi Harada. Phase-field simulation with the CALPHAD method for the microstructure evolution of multi-component Ni-base superalloys. *Intermetallics*, 16(2):239–245, February 2008. [16](#)
- [44] Alpha A Lee, Andreas Münch, and Endre Süli. Degenerate mobilities in phase field models are insufficient to capture surface diffusion. *Applied Physics Letters*, 107(8):081603, 2015. [3](#)
- [45] Alpha Albert Lee, Andreas Munch, and Endre Suli. Sharp-interface limits of the cahn–hilliard equation with degenerate mobility. *SIAM Journal on Applied Mathematics*, 76(2):433–456, 2016. [3](#)
- [46] Hyun Geun Lee, Jeong-Whan Choi, and Junseok Kim. A practically unconditionally gradient stable scheme for the N-component Cahn–Hilliard system. *Physica A: Statistical Mechanics and its Applications*, 391(4):1009–1019, February 2012. [16](#), [17](#)
- [47] Hyun Geun Lee and Junseok Kim. A second-order accurate non-linear difference scheme for the N -component Cahn–Hilliard system. *Physica A: Statistical Mechanics and its Applications*, 387(19-20):4787–4799, August 2008. [16](#), [17](#)
- [48] X Li, J Lowengrub, A Ra Tz, and A Voigt. SOLVING PDES IN COMPLEX GEOMETRIES: A DIFFUSE DOMAIN APPROACH. page 27. [25](#)
- [49] Yibao Li, Jung-Il Choi, and Junseok Kim. Multi-component Cahn–Hilliard system with different boundary conditions in complex domains. *Journal of Computational Physics*, 323:1–16, October 2016. [16](#)
- [50] Yibao Li, Darae Jeong, Jaemin Shin, and Junseok Kim. A conservative numerical method for the Cahn–Hilliard equation with Dirichlet boundary conditions in complex domains. *Computers & Mathematics with Applications*, 65(1):102–115, January 2013. [25](#)
- [51] Chun Liu and Jie Shen. A phase field model for the mixture of two incompressible fluids and its approximation by a fourier-spectral method. *Physica D: Nonlinear Phenomena*, 179(3-4):211–228, 2003. [26](#)
- [52] Francesco Maggi. *Sets of finite perimeter and geometric variational problems: an introduction to Geometric Measure Theory*. Number 135. Cambridge University Press, 2012. [1](#)
- [53] Barry Merriman, James Kenyard Bence, and Stanley Osher. *Diffusion generated motion by mean curvature*. Department of Mathematics, University of California, Los Angeles, 1992. [27](#)
- [54] Stefan Metzger. On numerical schemes for phase-field models for electrowetting with electrolyte solutions. *PAMM*, 15(1):715–718, 2015. [26](#)
- [55] Frank Morgan. Lowersemicontinuity of energy clusters. *Proceedings of the Royal Society of Edinburgh Section A: Mathematics*, 127(4):819–822, 1997. [1](#)
- [56] Meher Naffouti, Rainer Backofen, Marco Salvalaglio, Thomas Bottein, Mario Lodari, Axel Voigt, Thomas David, Abdelmalek Benkouider, Ibtissem Fraj, Luc Favre, et al. Complex dewetting scenarios of ultrathin silicon films for large-scale nanoarchitectures. *Science advances*, 3(11):eaao1472, 2017. [3](#)
- [57] Robert L Pego. Front migration in the nonlinear cahn–hilliard equation. *Proceedings of the Royal Society of London. A. Mathematical and Physical Sciences*, 422(1863):261–278, 1989. [3](#)
- [58] Andreas Rätz, Angel Ribalta, and Axel Voigt. Surface evolution of elastically stressed films under deposition by a diffuse interface model. *Journal of Computational Physics*, 214(1):187–208, 2006. [3](#)

- [59] Marco Salvalaglio, Rainer Backofen, Roberto Bergamaschini, Francesco Montalenti, and Axel Voigt. Faceting of equilibrium and metastable nanostructures: a phase-field model of surface diffusion tackling realistic shapes. *Crystal Growth & Design*, 15(6):2787–2794, 2015. [3](#)
- [60] Marco Salvalaglio, Rainer Backofen, Axel Voigt, and Francesco Montalenti. Morphological evolution of pit-patterned si (001) substrates driven by surface-energy reduction. *Nanoscale research letters*, 12(1):554, 2017. [3](#)
- [61] Marco Salvalaglio, Maximilian Selch, Axel Voigt, and Steven Wise. Doubly degenerate diffuse interface models of anisotropic surface diffusion. 04 2020. [16](#)
- [62] Marco Salvalaglio, Axel Voigt, and Steven M Wise. Doubly degenerate diffuse interface models of surface diffusion. *arXiv preprint arXiv:1909.04458*, 2019. [3](#), [16](#)
- [63] Jie Shen, Xiaofeng Yang, and Haijun Yu. Efficient energy stable numerical schemes for a phase field moving contact line model. *Journal of Computational Physics*, 284:617–630, 2015. [26](#)
- [64] Jaemin Shin, Darae Jeong, and Junseok Kim. A conservative numerical method for the Cahn–Hilliard equation in complex domains. *Journal of Computational Physics*, 230(19):7441–7455, August 2011. [25](#)
- [65] Jaemin Shin, Hyun Geun Lee, and June-Yub Lee. First and second order numerical methods based on a new convex splitting for phase-field crystal equation. *J. Comput. Phys.*, 327:519–542, 2016. [16](#)
- [66] Jaemin Shin, Hyun Geun Lee, and June-Yub Lee. Unconditionally stable methods for gradient flow using convex splitting Runge-Kutta scheme. *J. Comput. Phys.*, 347:367–381, 2017. [16](#)
- [67] David N Sibley, Andreas Nold, Nikos Savva, and Serafim Kalliadasis. The contact line behaviour of solid-liquid-gas diffuse-interface models. *Physics of Fluids*, 25(9):092111, 2013. [26](#)
- [68] David N Sibley, Andreas Nold, Nikos Savva, and Serafim Kalliadasis. On the moving contact line singularity: Asymptotics of a diffuse-interface model. *The European Physical Journal E*, 36(3):26, 2013. [26](#)
- [69] Knut Erik Teigen, Xiangrong Li, John Lowengrub, Fan Wang, and Axel Voigt. A DIFFUSE-INTERFACE APPROACH FOR MODELING TRANSPORT, DIFFUSION AND ADSORPTION/DESORPTION OF MATERIAL QUANTITIES ON A DEFORMABLE INTERFACE. page 29. [25](#)
- [70] Alessandro Turco, François Alouges, and Antonio DeSimone. Wetting on rough surfaces and contact angle hysteresis: numerical experiments based on a phase field model. *ESAIM: Mathematical Modelling and Numerical Analysis-Modélisation Mathématique et Analyse Numérique*, 43(6):1027–1044, 2009. [26](#)
- [71] Dong Wang, Xiao-Ping Wang, and Xianmin Xu. An improved threshold dynamics method for wetting dynamics. *Journal of Computational Physics*, 392:291–310, 2019. [27](#)
- [72] Xiaoyu Wei, Shidong Jiang, Andreas Kloeckner, and Xiao-Ping Wang. An integral equation method for the cahn-hilliard equation in the wetting problem. *Journal of Computational Physics*, page 109521, 2020. [26](#)
- [73] S. M. Wise, C. Wang, and J. S. Lowengrub. An energy-stable and convergent finite-difference scheme for the phase field crystal equation. *SIAM J. Numer. Anal.*, 47(3):2269–2288, 2009. [16](#)
- [74] Xianmin Xu, Wenjun Ying, Xiaoqin Shen, Qian Yang, Lin Bai, Kaitai Li, Jie Du, Eric Chung, Zhi-Qin John Xu, Yaoyu Zhang, et al. An adaptive threshold dynamics method for three-dimensional wetting on rough surfaces. *preprint*, 2019. [27](#)
- [75] Junxiang Yang and Junseok Kim. An unconditionally stable second-order accurate method for systems of Cahn–Hilliard equations. *Communications in Nonlinear Science and Numerical Simulation*, 87:105276, August 2020. [16](#), [17](#), [25](#)
- [76] Thomas Young. Iii. an essay on the cohesion of fluids. *Philosophical transactions of the royal society of London*, (95):65–87, 1805. [1](#), [26](#)
- [77] Shiwei Zhou and Michael Yu Wang. Multimaterial structural topology optimization with a generalized Cahn–Hilliard model of multiphase transition. *Struct Multidisc Optim*, 33(2):89–111, December 2006. [16](#)
- [78] Jingzhi Zhu, Long-Qing Chen, Jie Shen, and Veena Tikare. Coarsening kinetics from a variable-mobility cahn-hilliard equation: Application of a semi-implicit fourier spectral method. *Phys. Rev. E*, 60:3564–3572, Oct 1999. [17](#)

UNIV LYON, INSA DE LYON, CNRS UMR 5208, INSTITUT CAMILLE JORDAN, 20 AVENUE ALBERT EINSTEIN, F-69621 VILLEURBANNE, FRANCE, ELIE.BRETIN@INSA-LYON.FR

UNIV LYON, UNIVERSITÉ CLAUDE BERNARD LYON 1, CNRS UMR 5208, INSTITUT CAMILLE JORDAN, 43 BOULEVARD DU 11 NOVEMBRE 1918, F-69622 VILLEURBANNE, FRANCE, DENIS@MATH.UNIV-LYON1.FR

UNIV LYON, UNIVERSITÉ CLAUDE BERNARD LYON 1, CNRS UMR 5208, INSTITUT CAMILLE JORDAN, 43 BOULEVARD DU 11 NOVEMBRE 1918, F-69622 VILLEURBANNE, FRANCE, MASNOU@MATH.UNIV-LYON1.FR

UNIV LYON, UNIVERSITÉ CLAUDE BERNARD LYON 1, CNRS UMR 5208, INSTITUT CAMILLE JORDAN, 43 BOULEVARD DU 11 NOVEMBRE 1918, F-69622 VILLEURBANNE, FRANCE, SENGERS@MATH.UNIV-LYON1.FR

UNIV LYON, UNIVERSITÉ CLAUDE BERNARD LYON 1, CNRS UMR 5208, INSTITUT CAMILLE JORDAN, 43 BOULEVARD DU 11 NOVEMBRE 1918, F-69622 VILLEURBANNE, FRANCE, TERII@MATH.UNIV-LYON1.FR